Use of Ligand Steric Properties to Control the Thermodynamics and Kinetics of Oxidative Addition and Reductive Elimination with Pincer-ligated Rh Complexes

Shunyan Gu[†], Robert J. Nielsen[‡*], Kathleen H. Taylor[†], George C. Fortman[†], Junqi Chen[†], Diane A. Dickie[†], William A. Goddard III[‡*], T. Brent Gunnoe[†*]

[†]Department of Chemistry, University of Virginia, Charlottesville, VA 22904

[‡]Materials and Process Simulation Center, Department of Chemistry, California Institute of Technology, Pasadena, CA 91125

robert.smith.nielsen@gmail.com, wag@caltech.edu, tbg7h@virginia.edu

ABSTRACT

Oxidative addition and reductive elimination reactions are central steps in many catalytic processes, and controlling the energetics of reaction intermediates is key to enabling efficient catalysis. A series of oxidative addition and reductive elimination reactions using (^{R}PNP)RhX complexes (R = *tert*-butyl, *iso*-propyl, mesityl and phenyl; X = Cl, I) was studied to deduce the impact of the size of the phosphine substituents. Using (^{R}PNP)RhCl as starting material, oxidative addition of MeI was observed to produce (^{R}PNP)Rh(Me)(I)Cl, which was followed by reductive elimination of MeCl to form (^{R}PNP)RhI. The thermodynamics and kinetics vary with the identity of the substituent "R" on phosphorus of the PNP ligand. The presence of large steric bulk (e.g., R = *tert*-butyl, mesityl) on the phosphine favors Rh(I) compared to the presence of two smaller substituents (e.g., R = *iso*-propyl, phenyl). An Eyring plot for the oxidative addition of MeI to (^{tBu}PNP)RhCl in THF-d_8 is consistent with a polar two-step reaction pathway, and the formation of [(^{tBu}PNP)Rh(Me)I]I is also consistent with this mechanism. DFT calculations show steric bulk affects the reaction energies of addition reactions that generate six-coordinate complexes by tens of kcal·mol^{-1}. Ligand steric bulk is calculated to have a reduced effect (a few kcal·mol^{-1}) on S_N2 addition barriers, which only require access to one side of the square plane.

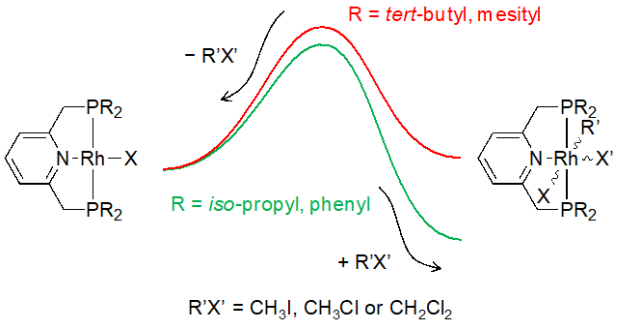

INTRODUCTION

Oxidative addition and reductive elimination transformations provide reactions that break and form bonds. These fundamental reactions are incorporated into many catalytic processes. For example, they are key reactions in catalytic C–C coupling reactions.[1-6] As a result, understanding how the features of the catalyst (e.g., metal identity, metal oxidation state, ligand donor ability, ligand steric parameters) dictate the energetics of oxidative addition and reductive elimination reactions is critical to understanding catalyst activity for better catalysis design. In particular, understanding energy profiles of catalytic intermediates is important to designing molecular catalysts for light alkane partial oxidations.[7-16]

Given the inert nature of alkanes, their selective functionalization is a substantial challenge.[9-11,17-20] Since Shilov's discovery on Pt-mediated alkane functionalization,[8,21,22] electrophilic late metal complexes have been developed for catalyzing the functionalization of alkanes.[8-16,21-26] A significant limitation of this approach is the ability of weakly basic solvents to coordinate to the metal and inhibit catalyst activity.[27-29] While several electrophilic catalysts are efficient for methane functionalization in superacidic oleum (H_2SO_4 + SO_3), they are less or not active in more weakly acidic solvents.[7] A possible strategy is to use earlier transition metals, such as those based on Rh or Ir, which are anticipated to be less electrophilic.[30,31] Using a putative catalytic cycle that mirrors the proposed Pt(II)/Pt(IV) cycle of Pt-catalyzed Shilov type reactions, a Rh catalytic cycle would involve C–H oxidative addition to Rh(I) to form a Rh(III) intermediate followed by reductive elimination of the Rh^{III}–R bond (Scheme 1). Thus, regardless of the specific mechanistic details, a key step in rhodium catalyzed alkane functionalization using Shilov-type chemistry is the reductive elimination of RX (X = halide or pseudo-halide) from an X–Rh^{III}–R intermediate (Scheme 2).[12,32] While C–H activation by Rh^{I} complexes has been reported,[33-42]

examples of reductive elimination of alkyl halide from Rh^{III} complexes are not common.[43-47]

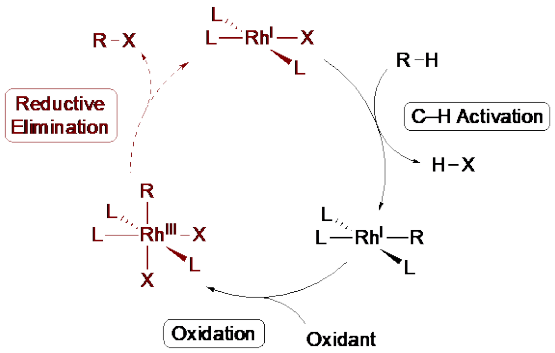

Scheme 1. Possible Shilov type catalytic cycle for Rh catalyzed hydrocarbon C–H functionalization.[22,48]

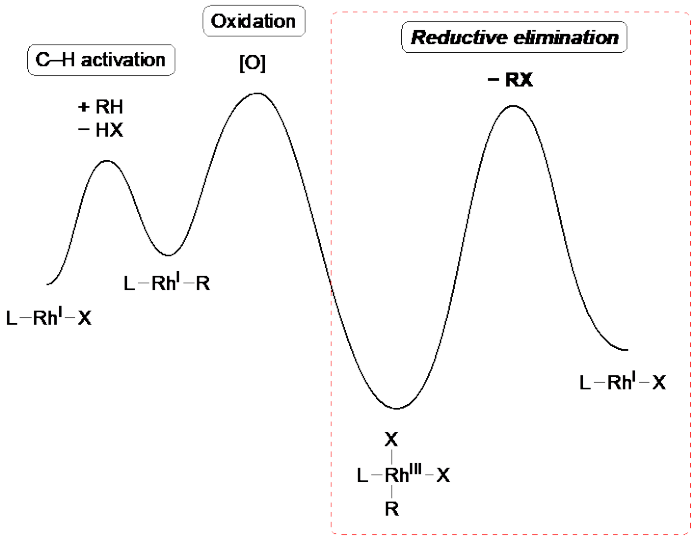

Scheme 2. General energy diagram of Rh-mediated hydrocarbon functionalization that operates via a Rh^{I}/Rh^{III} pathway (note: relative energetics are based on unpublished calculations of several Rh complexes). The Rh^{III} intermediate can be thermodynamically favored resulting in a high activation barrier for the reductive elimination of RX (in the red box).

In addition to alkane functionalization, reductive elimination reactions are important in industrial processes such as methanol carbonylation and olefin hydroformylation.[49-53] In non-radical reductive elimination, S_N2 (polar two-step) and concerted mechanisms are the two most common pathways (Scheme 3).[54-58] In the S_N2 pathway, a charged intermediate is commonly formed upon dissociation of an anionic ligand from the metal center. This two-step mechanism is often accelerated in polar solvents,

where the intermediate can be stablized. In the concerted pathway, a three-center transition state is typically invoked.

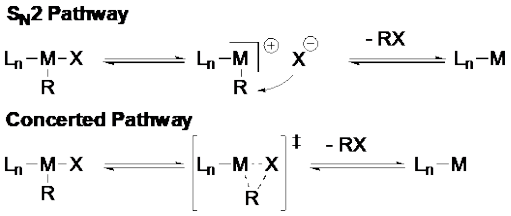

Scheme 3. Common pathways for reductive elimination of RX from a metal center (R = hydrocarbyl and X = formally anionic species such as hydride, hydrocarbyl, halide, etc.).[56,58]

Some recent reports have focused on reductive elimination reactions from Rh^{III}, Pd^{IV}, Pt^{IV} and Au^{III} complexes.[43,45,59-62] The Milstein group has reported on mechanistic studies with a focus on ligand influence for reductive elimination of MeX (X = halide of pseudo halide) from Rh^{III} complexes ligated by both PCP ligands and PNP ligands.[43-45] With our recent reports of Rh-mediated C–H activation and functionalization,[38,63-70] we have become interested in understanding how to modify ligands to control the energetics of redox bond-breaking and bond-forming processes that convert between Rh^{I}, Rh^{II}, Rh^{III} and Rh^{IV}.[64] Although understanding ligand effects on reductive eliminations can be more subtle than σ-donor effects,[71,72] one strategy to shift Rh^{I}/Rh^{III} equilibria toward Rh^{I} is to alter metal electron density based on ligand donor ability. For example, our group studied reductive elimination from a series of (^{R}terpy)Rh(Me)(Cl)(I) complexes (R = *tert*-butyl, NO_2) in acidic media where the electron-withdrawing nitro group facilitates reductive elimination of the methyl ligand.[46,47] Most relevant here, steric effects could also be used to facilitate two-electron reductive eliminations from octahedral d^6 Rh^{III} complexes to form square planar d^8 Rh^{I} complexes, where Rh^{III} complexes can be destablized with bulky ligands. For example, "axial steric bulk," which is defined as the ligand sterics above/below the coordination plane

of a square planar complex, could be used to destabilize octahedral Rh^{III} complexes relative to square planar Rh^{I} complexes. PNP pincer ligands, which provide a tridentate binding mode, offer an opportunity to control axial steric bulk based on phosphine substituents (Figure 1). Examples are known where steric factors are central in reactions of pincer ligated transition metal complexes.[44,45,73-76] With interest in controlling the thermodynamics of bond-breaking/forming reactions that cycle through formal $Rh^{III/I}$ oxidation states as a means to potentially optimize kinetics of catalytic reactions, we have investigated the axial steric effect on oxidative addition and reductive elimination reactions of a series of (^{R}PNP)Rh (^{R}PNP = 2,6-bis-(di-hydrocarbylphosphinomethyl)pyridine) complexes with various steric bulk (Scheme 4). Initial computational modeling studies suggested that large substituents on the phosphine ligands would favor, thermodynamically and kinetically, square planar Rh^{I} complexes over octahedral Rh^{III} complexes. Experimental studies are consistent with this hypothesis. Herein, we report the details of these combined computational/experimental studies.

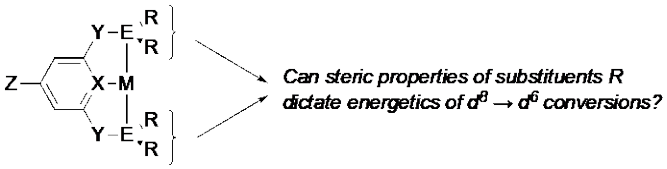

Figure 1. Generic structure of a metal complex with a "pincer" ligand where substituents R can be modified to control steric profile.

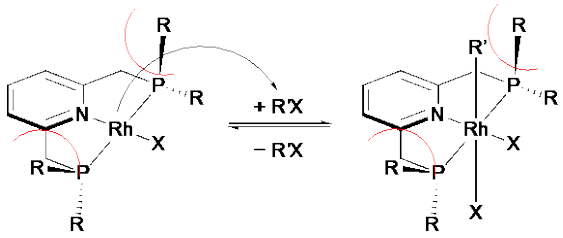

Scheme 4. Destabilization of octahedral Rh^{III} complexes by tuning "axial steric bulk" in (^{R}PNP)Rh complexes (R = *tert*-butyl, *iso*-propyl, mesityl and phenyl).

RESULTS AND DISCUSSION

Density functional theory calculations were used to predict ΔG and $\Delta G^{\ddagger}$ for the elimination of CH_3X products from (^{R}PNP)Rh(Me)$(X)_2$ intermediates in order to gauge the likelihood of extending this transformation from catalytic cycles based on more electrophilic metals to rhodium. Sterically unencumbered and electron-deficient pincer ligands have been observed to form multinuclear[77,78] or *fac*-coordinated complexes[79]. Nonetheless we modeled R = Me, CF_3 and *tert*-butyl variants as *mer* pincer complexes to isolate the steric effects of larger phosphine substituents and to assess what free energy surfaces might be afforded by a more diverse set of ligands.

The R = methyl cases show that elimination is not kinetically or thermodynamically favorable if steric or electronic factors are not specifically employed to drive the reaction (Scheme 5). Consistent with this, reductive elimination of methyl halides from (PNP)Rh^{III} complexes has previously been observed when trapping agents (e.g., CO) are included to sequester Rh^{I} or CH_3X products,[45] a tactic incompatible with catalytic cycles. Oxygen-based nucleophiles such as trifluoroacetate and water offer advantages over halides in C–H activation reactions since their basicity in polar media drives the removal of protons from hydrocarbons. However, these harder nucleophiles lead to higher S_N2 elimination barriers than iodide. Increasing the size of the phosphine substituent to *tert*-butyl imparts an additional 20 kcal·mol^{-1} driving force to the elimination of methyl trifluoroacetate, while the barrier is reduced by 1.4 kcal·mol^{-1}. Rendering the rhodium center more electrophilic via the trifluoromethyl phosphine substituents benefits both the activation barrier and reaction energy of elimination, making the elimination of methanol and

methyl trifluoroacetate exergonic. Predicted activation barriers range from roughly 30 to 40 kcal·mol^{-1}, and only reactions at the low end of this range are suitable for hydrocarbon functionalization cycles even at temperatures high for homogeneous catalysis. The steric and electronic properties of the ligand and nucleophile must therefore be limited by this constraint.

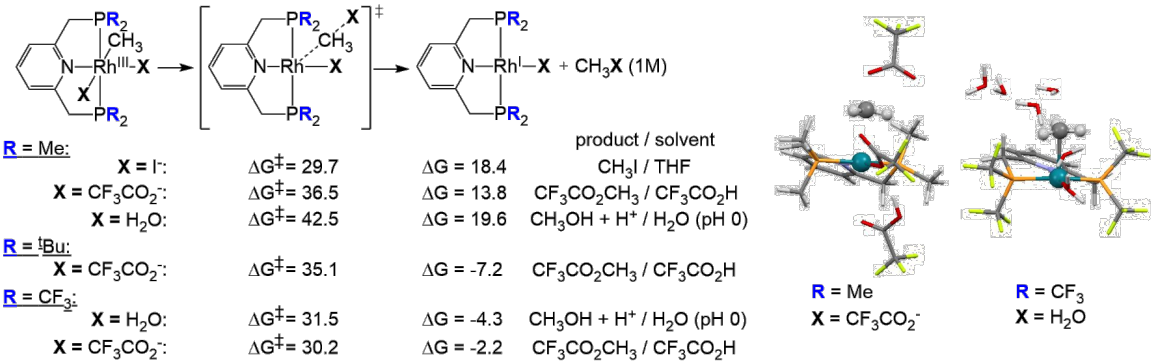

Scheme 5. Computed activation and reaction free energies (kcal·mol^{-1} at 298 K) for S_N2 elimination reactions from Rh^{III} methyl complexes. Representative transition state structures with explicit solvent molecules are shown on the right with the Rh-CH_3 unit represented by spheres.

Based on these computational modeling results, in this work, we sought to quanitfy, experimentally and computationally, the impact of the axial steric effect on oxidative addition and reductive elimination reactions for this series of pincer ligated Rh complexes. Multiple small molecules were tested, and MeI and CH_2Cl_2 were chosen as suitable substrates due to clean reactivity.

Tert-butyl and mesityl were selected as the larger phosphine substituents while *iso*-propyl and phenyl were selected as the smaller substituents allowing for the comparison of both alkyl groups and aryl groups. Although there is not a model that can perfectly quantify axial steric bulkiness, the solid-G software is able to visualize the shielding of different phosphine substituents perpendicular to the square plane centered around Rh (Table 1).[80] This analysis, based on structures obtained from single-crystal X-ray diffaction, provides a view of the steric shielding above/below the Rh square plane. The

visualization of steric shielding is shown in rows 4 and 6 of Table 1, where the blue indicates area blocked by the PNP ligand. Compared with (^{iPr}PNP)RhCl and (^{Ph}PNP)RhCl, as expected, (^{tBu}PNP)RhCl and (^{Mes}PNP)RhCl have larger ligand shielding (blue area) of the Rh center.

Table 1. Crystal structures (top) of (^{tBu}PNP)RhCl (**1a**), (^{iPr}PNP)RhCl (**2a**), (^{Mes}PNP)RhCl (**3a**) and (^{Ph}PNP)RhCl (**4a**), and the visualization of shielding of different ligands on Rh center (bottom). The ^{R}PNP ligand shieldings are indicated in blue, and the Cl contributions are indicated in red. In (^{Mes}PNP)RhCl, since there is no C_2 symmetry in the crystal structure, the shielding is different from above and below the square plane in the crystal structure. Thus, two images are provided.[80-82]

Phosphine substituent			
***tert*-butyl**[a]	***iso*-propyl**[a]	**mesityl**	**phenyl**[a]
ORTEP			
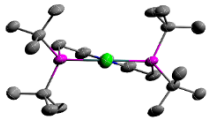		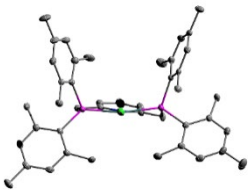	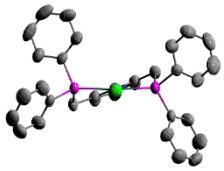
Ligand shielding on Rh center			
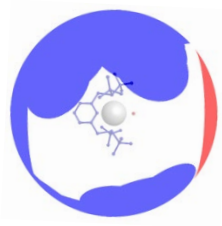	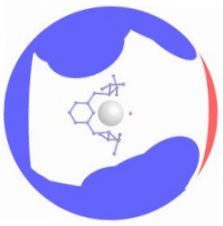	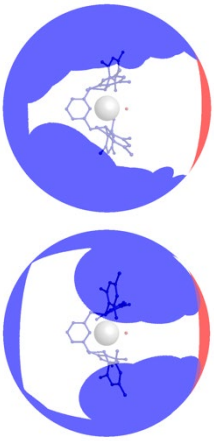	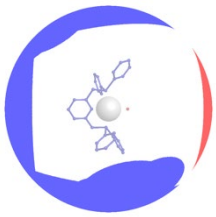

[a] The crystal structure has been previously reported.[80-82]

Reactions of (^{tBu}PNP)RhCl (1a). The complex (^{tBu}PNP)RhCl (**1a**) was prepared by mixing ^{tBu}PNP and $[Rh(\mu\text{-}C_2H_4)_2Cl]_2$ in THF according to a published procedure.[83] In a THF solution of **1a**, MeI was added dropwise. With increasing amount of added MeI, an orange precipitate was formed, which was found to be consistent with the reported NMR spectra of [(^{tBu}PNP)Rh(Me)I]I (**1d'**).[44] *In situ* observation

of the reaction of **1a** with MeI by ^{1}H NMR spectroscopy indicates that **1a** undergoes oxidative addition to generate a Rh^{III} complex as an intermediate that quickly eliminates MeCl to form (^{tBu}PNP)RhI (**1c**) (Figures 2, 3) and MeCl. With excess MeI added to **1c**, an equilibrium between **1c**, MeI and **1d'** was established (Scheme 6). The Rh^{III} intermediate was not successfully isolated, but NMR data are consistent with the expected oxidative addition product (^{tBu}PNP)Rh(Me)(Cl)(I). A doublet with $^{1}J_{RhP}$ of 101 Hz was observed in the $^{31}P\{^{1}H\}$ NMR spectrum, indicating the formation of Rh^{III} species.[84,85] Two diastereotopic PCH_2 peaks were observed at 4.39 and 4.02 ppm in the ^{1}H NMR spectrum, indicating the loss of a mirror plane. Attempts to generate **1b** *in situ* were made by charging MeCl to THF solutions of **1c**, but no reaction was observed, indicating that the Rh^{I} species **1c** is likely favored thermodynamically over **1b**.

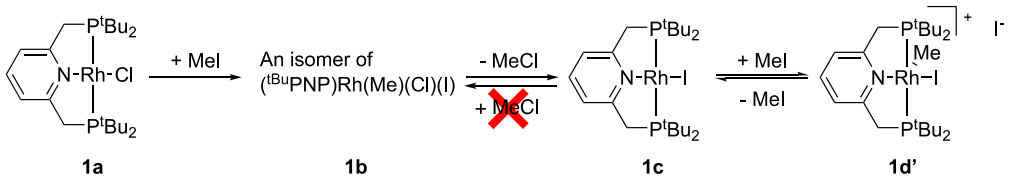

Scheme 6. Oxidative addition and reductive elimination reactions using (^{tBu}PNP)RhCl (**1a**) as the starting complex. All the reactions were performed in THF. **1b** is a proposed structure without specifying the exact isomer.

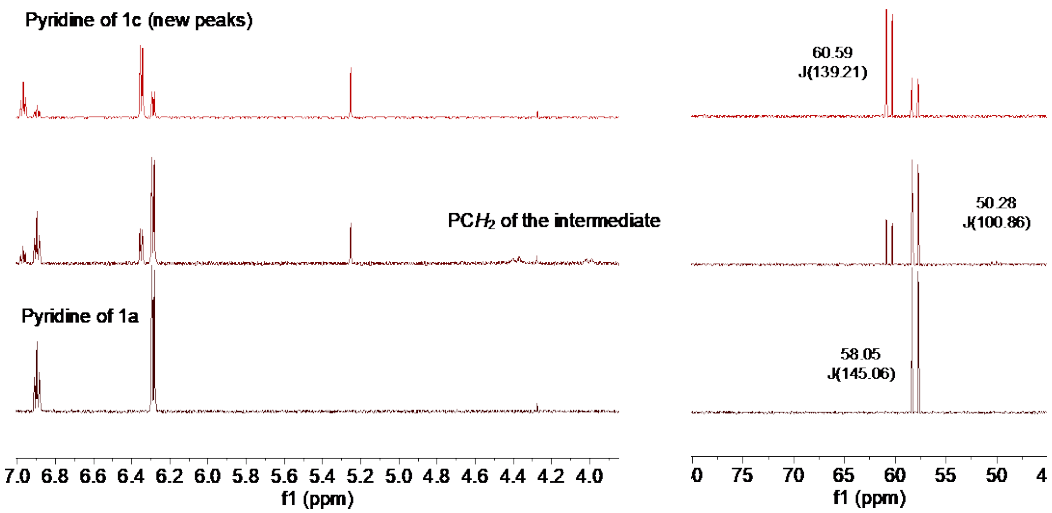

Figure 2. ^{1}H NMR (left) and ^{31}P{^{1}H} NMR (right) spectra of the reaction of (^{tBu}PNP)RhCl (**1a**) and MeI to form (^{tBu}PNP)RhI (**1c**) in C_6D_6 (from bottom to top: without MeI, 15 min, 50 min). Within 15 minutes of MeI addition (second from the bottom), the Rh^{III} complex, (^{tBu}PNP)Rh(Me)(Cl)(I), was observed at 50.3 ppm in ^{31}P{^{1}H} NMR with $^{1}J_{PRh}$ = 101 Hz.

Complex **1c** has been characterized by a single X-ray diffraction study (Figure 3). There is only slight difference in the bond lengths and bond angles between **1c** and the previously reported structure of **1a**.[81] In **1a**, the N–Rh bond length is 2.036(3) Å, while the same bond distance for **1c** is 2.049(6) Å.

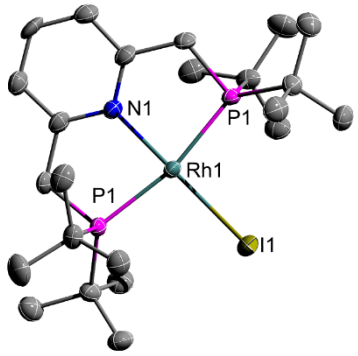

Figure 3. ORTEP of (^{tBu}PNP)RhI (**1c**). Ellipsoids are drawn at 50% probability level and hydrogen atoms are omitted for clarity. Selected bond lengths for **1c** (Å): Rh1–N1 2.049(6), Rh1–P1 2.2815(16), Rh1–P1 2.2815(16), Rh1–I1 2.6077(8). Selected bond angles for **1c** (°): N1–Rh1–P1 83.49(4), N1–Rh1–P2 83.49(4), P1–Rh1–P2 166.99(8), N1–Rh1–I1 180.00(2), P1–Rh1–I1 96.51(4), P2–Rh1–I1 96.51(4).

The kinetics of reaction between **1a** and MeI were probed from 27 °C to 54 °C. The concentrations of **1a** and MeI were monitored with respect to time using integration of ^{1}H NMR spectra (Figure 4). The

results demonstrate a good fit to a second order reaction, first order in both **1a** and MeI, according to eq 1. The k_{obs} was determined to be 6.2(5) × 10^{-3} $M^{-1}\cdot s^{-1}$ at 300 K, which corresponds to a $\Delta G^{\ddagger}$ of 20.6 $kcal\cdot mol^{-1}$.

$$\frac{1}{[A]_0-[B]_0}\ln\frac{[A]}{[B]} = kt + \ln\frac{[A]_0}{[B]_0} \quad (1)$$

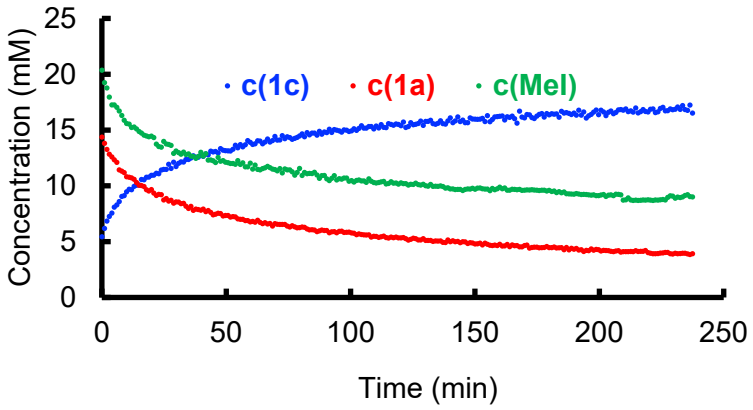

Figure 4. Concentration changes for (^{tBu}PNP)RhCl (**1a**), MeI and (^{tBu}PNP)RhI (**1c**) with respect to time. Conditions: 0.5 mL THF-d_8, 16 mM (^{tBu}PNP)RhCl (**1a**), 20 mM MeI, HMDSO (hexamethyldisiloxane) as the internal standard, 319 K.

An Eyring plot was obtained using variable temperature NMR experiments from 27 °C to 54 °C (Figure 5). The Eyring plot gives a good linear fit, and the $\Delta H^{\ddagger}$ and $\Delta S^{\ddagger}$ of the reaction were determined as 10.4(8) $kcal\cdot mol^{-1}$ and −34(2) $cal\cdot mol^{-1}\cdot K^{-1}$, respectively. The large and negative $\Delta S^{\ddagger}$ is consistent with a S_N2-type mechanism with a five-coordinate square pyramidal complex forming as an intermediate (Scheme 7).[45,86] The proposed structure, [(^{tBu}PNP)Rh(Me)(Cl)](I) (**1b'**), is consistent with the reported crystal structure of **1d'**, which also has a five-coordinate square pyramidal structure with one iodide appearing as a counter ion.[44] This might be due to the large axial steric bulk, which could prevent iodide from bonding with the Rh center, and it also applies to the case of the intermediate, [(^{tBu}PNP)Rh(Me)(Cl)](I) (**1b'**).

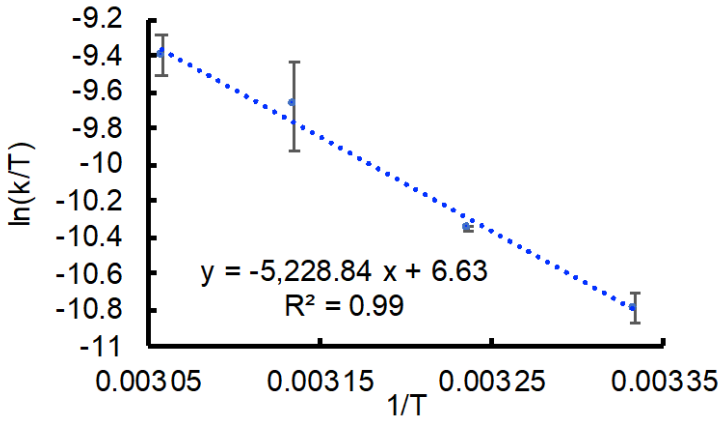

Figure 5. Eyring plot for the oxidative addition of MeI to (^{tBu}PNP)RhCl (**1a**). All data points and standard deviations are the results of at least three independent experiments.

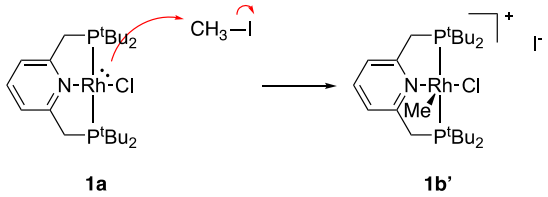

Scheme 7. Proposed S_N2-type mechanism for the oxidative addition of MeI to (^{tBu}PNP)RhCl (**1a**).

Due to the low solubility of **1d'** in THF-d_8, determination of the equilibrium constant as a function of temperature between **1c**/MeI and **1d'** was performed in CD_2Cl_2. The equilibrium constant of this reaction, at 27 °C, is 78(7) (Note: the K_{eq} and standard deviation are the result of three independent experiments). Using the variable temperature data and experimentally determined K_{eq} values, a van't Hoff plot was created (Figure 6). The ΔH and ΔS of the reaction were calculated to be −15.2(6) kcal·mol^{-1} and −42(2) cal·mol^{-1}·K^{-1}, respectively.

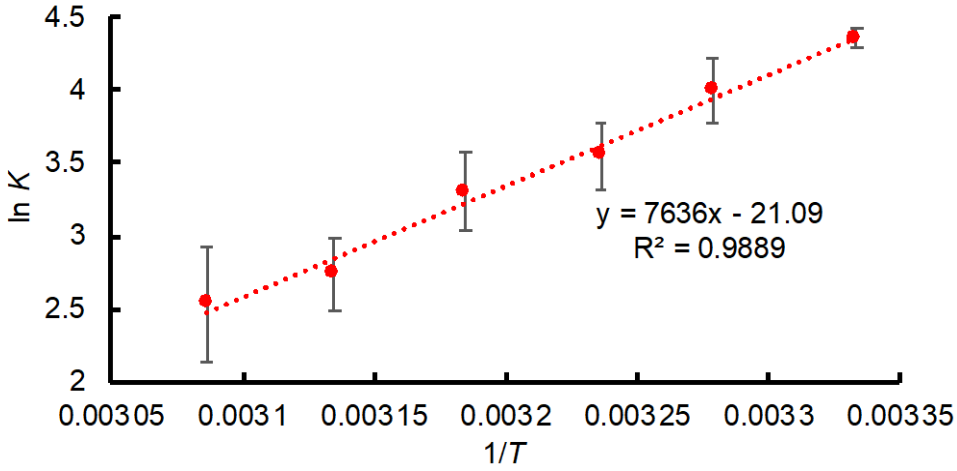

Figure 6. The van't Hoff plot of the equilibrium between (^{tBu}PNP)RhI (**1c**), MeI and [(^{tBu}PNP)Rh(Me)I]I (**1d'**). Conditions: 0.5 mL CD_2Cl_2, 12.6 mM **1d'**, HMDSO (hexamethyldisiloxane) in C_6D_6 in a capillary as the internal standard, 300 K – 324 K. All data points and standard deviations are the results of at least three independent experiments.

Reactions of (^{iPr}PNP)RhCl (2a). (^{iPr}PNP)RhCl (**2a**) was synthesized by mixing ^{iPr}PNP and [Rh(μ-$C_2H_4)_2Cl]_2$ in THF.[45] The reaction of MeI with **2a** in THF-d_8 generates two Rh^{III} complexes both exhibiting $^1J_{PRh}$ of 99 Hz in $^{31}P\{^1H\}$ NMR spectra. The identities of the complexes have been confirmed by X-ray crystallography to be isomers of (^{iPr}PNP)Rh(Me)(I)(Cl), and both isomers possess a methyl at the position *cis* to the pyridyl (**2b-1**, **2b-2**, Figure 7). The two isomers co-crystallize, with **2b-1** being the dominant isomer (**2b-1**:**2b-2** = 86:14). Complex **2b-1** has a chlorine atom *trans* to pyridyl N, giving a 173.0(2)° N–Rh–Cl bond angle, while **2b-2** shows a 98.0(3)° N–Rh–Cl bond angle. In the ^1H NMR spectrum of **2b-1** and **2b-2**, both complexes display C_s symmetry, as determined from the four peaks due to the isopropyl and the diastereotopic PCH_2 units.

We were unable to determine the rate of the oxidative addition of MeI to **2a** because the reaction is complete in < 10 minutes at −78 °C. An oxidative reaction experiment of **2a** and MeI using the same starting concentration as the reaction for **1a** (Figure 4) was performed in a screw cap NMR tube at −78 °C. After 10 min, **2a** was not observable by ^1H NMR spectroscopy. Assuming that reactions undergo

the same mechanism as for **1a** and **2a** and that more than 95% of the starting material was consumed by 10 min, a rate constant can be estimated to be ≥ 0.032 $M^{-1}\cdot s^{-1}$ at 195 K. Thus an upper limit on $\Delta G^{\ddagger}$ for this reaction can be estimated at ~13 $kcal\cdot mol^{-1}$. Heating a THF-d_8 solution of the mixture of **2b-1** and **2b-2** to 90 °C does not give the reductive elimination product (^{iPr}PNP)RhI (**2c**), and the product of MeCl reductive elimination followed by MeI oxidation addition, (^{iPr}PNP)Rh(Me)$(I)_2$, was not observed after 100 hours at 90 °C. Thus, in contrast to the ^{t}Bu variant **1b**, **2b** is stable against MeX (X = Cl, I) reductive elimination. (^{iPr}PNP)RhI (**2c**) was then synthesized independently by mixing **2a** and NaI in acetone.[87] Charging MeCl to a THF-d_8 solution of complex **2c** gives three isomers of **2b** according to NMR spectra.

The observations of reactivity of **1a** and **2a** are consistent with the hypothesis that reduced axial steric bulk stabilizes Rh^{III} relative to Rh^{I}, and the $\Delta G^{\ddagger}$ for reductive elimination from (^{iPr}PNP)Rh(Me)(Cl)(I) (**2b**) is larger than (^{tBu}PNP)Rh(Me)(Cl)(I) (**1b**). Mixing MeI with **2c** results in a rapid oxidative addition to form *trans*-(^{iPr}PNP)Rh(Me)I_2 (**2d**), turning the solution color from dark red to yellow (Scheme 8). The reaction of (^{tBu}PNP)RhI (**1c**) with MeI results in a rapid oxidative addition as well, however followed by immediate reductive elimination forming a rapid equilibrium between the two species. Compared with reaction of **1c**, the final product of **2c** oxidative addition (**2d**) is a six-coordinate Rh complex with both iodides binding to the Rh center. Assuming a similar mechanism as the reaction of **1c**, [(^{iPr}PNP)Rh(Me)I]I, with the *trans* position to the methyl vacant, might be an intermediate of the oxidative addition reaction. Heating a THF-d_8 solution of **2d** and 10 equivalents of CD_3I to 90 °C in a J Young Tube did not give the product of CD_3I exchange, (^{iPr}PNP)Rh$(CD_3)I_2$, after 7 days, indicating that reductive elimination of MeI from **2d** does not likely occur under this condition.

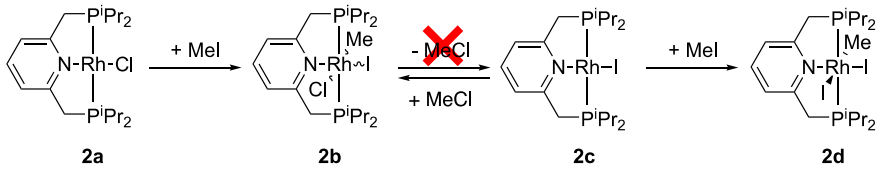

Scheme 8. Oxidative addition of MeI and MeCl using (^{iPr}PNP)RhCl (**2a**) and (^{iPr}PNP)RhI (**2c**) as the starting complexes. All the reactions were performed in THF. **2b** refers to a mixture of isomers of this complex.

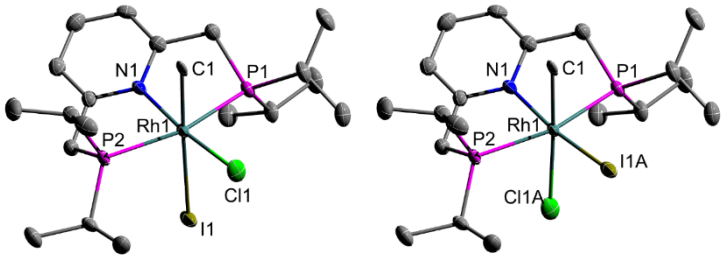

Figure 7. ORTEPs of two isomers of (^{iPr}PNP)Rh(Me)(I)(Cl) (**2b**; **2b-1** on the left, **2b-2** on the right), which are found as a co-crystallized mixture. Ellipsoids are drawn at 50% probability level and hydrogen atoms are omitted for clarity. Selected bond lengths for **2b** (Å): Rh1–N1 2.050(4), Rh1–C1 2.124(5), Rh1–P1 2.308(1), Rh1–P2 2.353(1). Selected bond lengths for **2b-1**: Rh1–Cl1 2.362(4), Rh1–I1 2.8424(6). Selected bond lengths for **2b-2**: Rh1–Cl1A 2.45(1), Rh1–I1A 2.460(8). Selected bond angles for **2b** (°): N1–Rh1–C1 87.2(2), N1–Rh1–P1 82.4(1), C1–Rh1–P1 86.8(1), N1–Rh1–P2 82.3(1), C1–Rh1–P2 91.0(1), P1–Rh1–P2 164.68(5). Selected bond angles for **2b-1** (°): N1–Rh1–Cl1 173.0(2), C1–Rh1–Cl1 86.2(2), P1–Rh1–Cl1 95.0(2), P2–Rh1–Cl1 100.0(2), N1–Rh1–I1 98.0(1), C1–Rh1–I1 174.8(1), P1–Rh1–I1 94.80(4), P2–Rh1–I1 88.79(3), Cl1–Rh1–I1 88.7(2). Selected bond angles for **2b-2** (°): N1–Rh1–Cl1A 98.0(3), C1–Rh1–Cl1A 171.3(4), P1–Rh1–Cl1A 100.8(4), P2–Rh1–Cl1A 82.8(4), N1–Rh1–I1A 172.1(2), C1–Rh1–I1A 85.3(2), P1–Rh1–I1A 94.7(2), P2–Rh1–I1A 100.3(2), Cl1A–Rh1–I1A 89.7(3).

Scheme 9 contains the calculated free energy surfaces for reactions of **1a** and **2a** with CH_3I in THF. The conversion of the Rh^I-Cl **1a** to Rh^I-I **1c** is accomplished by the S_N2 addition of CH_3I, rearrangement of halogen atoms, and S_N2 elimination of CH_3Cl. The immediate product of CH_3I addition is the five-coordinate ion pair **1b**, which is also predicted to be the most stable geometry for this Rh^{III} composition. The rearrangement that exchanges iodine and chlorine is slightly uphill (**1b-3**) and allows the reaction to proceed via CH_3Cl elimination. The octahedral intermediates **1b-2** and **1b-1** lie 6.1 and 14.5 kcal·mol^{-1} higher in free energy than **1b**, showing that the axial metal-halide bond is only metastable and that the

equitorial position is less hindered and better suited to host the larger iodide anion. We have not sought transition states for the halide rearrangement, but take the energy of the octahedral complexes to indicate that rearrangement may occur without barriers as high as the S_N2 reactions. The transition state for elimination of CH_3Cl (**TS2**, G = 21.4 kcal·mol^{-1}) is higher than that for CH_3I addition (**TS1**). We interpret that **TS2** is responsible for the effective barrier of $\Delta G^{\ddagger}$ = 20.6 kcal·mol^{-1} from experimental results (see above), and that the Rh^{III} intermediates are not observed spectroscopically because they are endergonic from the reactants.[88] Addition of another CH_3I molecule to **1c** proceeds with a geometry (**TS3**) and barrier similar to the first, yielding the five-coordinate **1d'**. An alternate pathway from **1b3** to **1d'** is intermolecular outersphere halide exchange; however, the observation of **1c** and MeCl is consistent with our proposed pathway. Since this addition is predicted to be endergonic, the reaction appears to be driven by Le Chatelier's principle and the precipitation of product. Computed thermochemistry (using the M06-L and B3PW91-d3 functionals) is compared to experimental data from this and related work[86] in order to estimate expected errors in the ESI.

We sought transition states for the elimination of CH_3Cl from **1b** with reductive elimination character. **TSRE-1** and **TSRE-2**, with free energies roughly 20 and 40 kcal·mol^{-1} higher than the S_N2-style **TS2**, may be described as migration of a methyl group along the Rh-Cl bond with coordination of the outer-sphere iodide. Such paths are apparently not kinetically relevant.

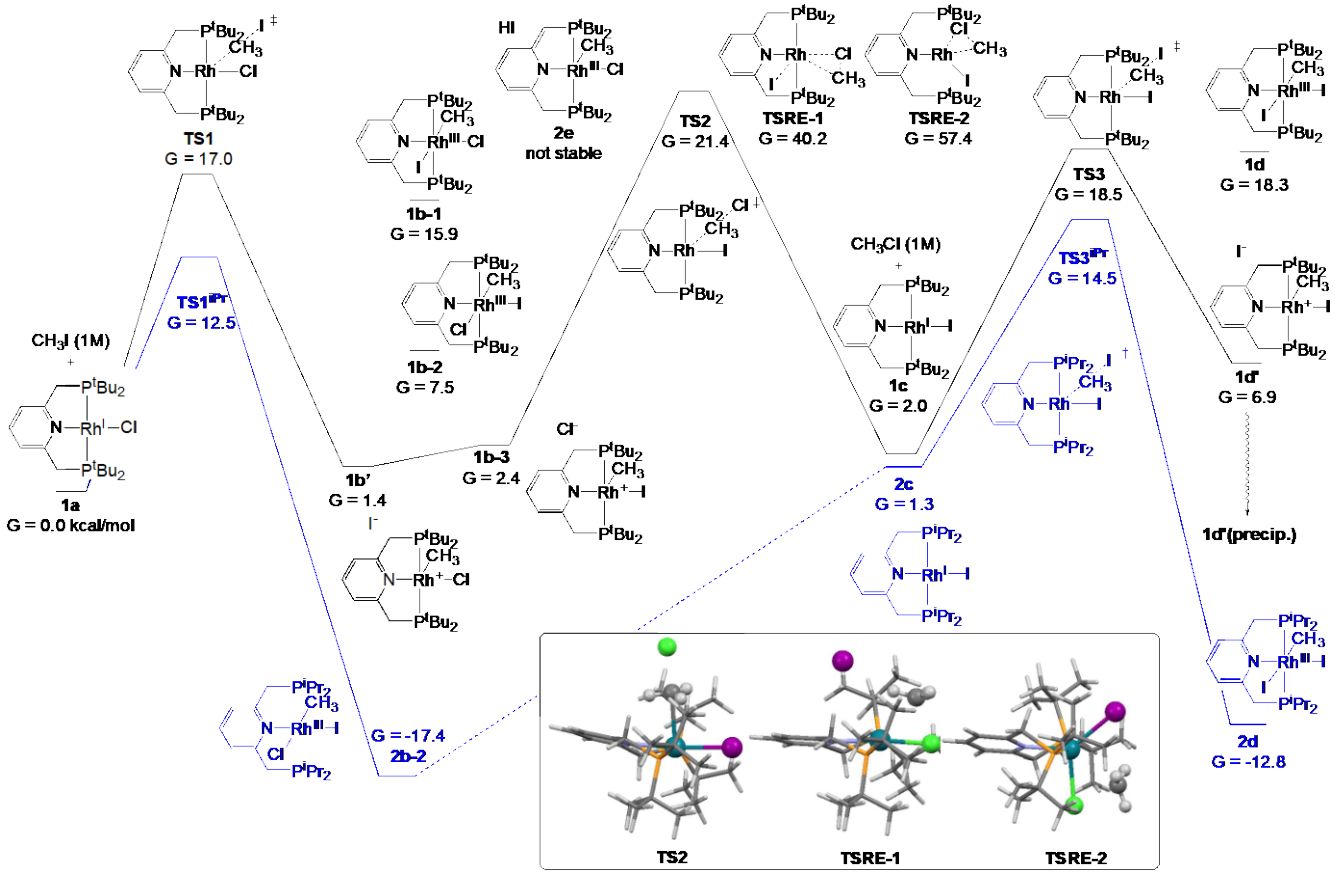

Scheme 9. Computed free energy surface (kcal·mol^{-1} at 298 K) for reactions of **1a** (in black) and **2a** (in blue) with CH_3I in THF. Inset shows the geometry of S_N2 and reductive elimination pathways for CH_3Cl elimination from **1b**.

When the *tert*-butyl phosphine substituents are replaced with *iso*-propyl groups, the activation barriers for addition of CH_3I to the square planar **2a** and **2b** are lowered by about 4 kcal·mol^{-1} from the analogous *tert*-butyl values. The dramatic difference between the two free energy surfaces is the stability of Rh^{III} states relative to Rh^{I}. The octahedral product of CH_3I addition **2b-2** is predicted to be 17.4 kcal·mol^{-1} exergonic, in contrast to the 7.5 kcal·mol^{-1} endergonic for **1b-2**. The octahedral (^{iPr}PNP)Rh(CH_3)(I)$_2$ complex **2d** is similarly stable. Furthermore, the five-coordinate ion pair (^{iPr}PNP)Rh(CH_3)(Cl)$^+$(I)$^-$ lies 12.3 kcal·mol^{-1} above the octahedral **2b-2** in free energy. The iodide ion prefers to be bound to Rh, in qualitative contrast to **1b'**. The (^{iPr}PNP)Rh^{III} states are thermodynamic

sinks, consistent with the lack of experimentally observed elimination reactions. In addition to being smaller than *tert*-butyl groups, the *iso*-propyl substituents can rotate to best accommodate each other and axial ligands as needed.

Reactions of (^{Mes}PNP)RhCl (3a). (^{Mes}PNP)RhCl (**3a**) was synthesized by stirring a THF solution of $[Rh(\mu\text{-}C_2H_4)_2Cl]_2$ and ^{Mes}PNP in a 1:2 ratio. ^{1}H NMR spectrum of **3a** indicates a molecule with four symmetry equivalent mesityl groups. The $^1J_{PRh}$ of 143 Hz for **3a** in the $^{31}P\{^1H\}$ NMR spectrum is consistent with a Rh^I oxidation state. To a THF solution of **3a**, MeI was added dropwise, resulting in a color change from red to yellow. Two Rh^{III} complexes were observed by $^{31}P\{^1H\}$ NMR spectroscopy each with $^1J_{PRh}$ = 99 Hz, indicating the likely formation of isomers of (^{Mes}PNP)Rh(Me)(I)(Cl) (**3b**). Stirring the yellow solution of the Rh^{III} products results in a color change back to red after ~30 min, and ^{1}H NMR and $^{31}P\{^1H\}$ NMR spectra are consistent with the formation of (^{Mes}PNP)RhI (**3c**) and another unidentified species as a minor product (Scheme 10). **3c** was synthesized independently by mixing **3a** and NaI in acetone, and the structure of **3c** was confirmed by X-ray crystallography (Figure 8). Monitoring the reaction by NMR spectroscopy indicates the formation of MeCl and CH_4.

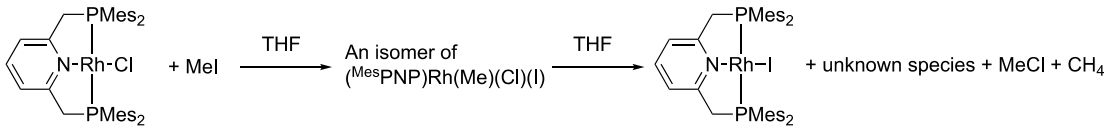

3a **3b** **3c**

Scheme 10. Oxidative addition MeI to (^{Mes}PNP)RhCl (**3a**) to form (^{Mes}PNP)Rh(Me)(I)(Cl) (**3b**) as a proposed intermediate and reductive elimination of MeCl to form (^{Mes}PNP)RhI (**3c**). An unidentified species and methane was also observed as the product. All the reactions were performed in THF.

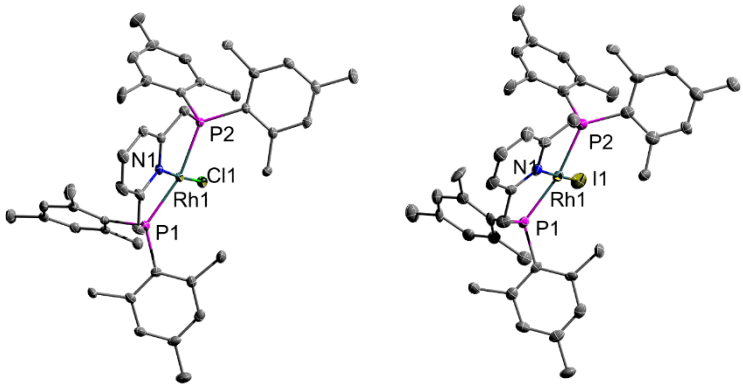

Figure 8. ORTEPs of (^{Mes}PNP)RhCl (**3a**, left) and (^{Mes}PNP)RhI (**3c**, right). Ellipsoids are drawn at 50% probability level and hydrogen atoms are omitted for clarity. Selected bond lengths for **3a** (Å): Rh1–N1 2.056(3), Rh1–P2 2.2703(9), Rh1–P1 2.2963(9), Rh1–Cl1 2.3757(8). Selected bond angles for **3a** (°): N1–Rh1–P2 84.66(9), N1–Rh1–P1 84.38(9), P2–Rh1–P1 164.43(3), N1–Rh1–Cl1 176.23(9), P2–Rh1–Cl1 92.43(3), P1–Rh1–Cl1 98.00(3). Selected bond lengths for **3c** (Å): Rh1–N1 2.053(9), Rh1–P1 2.281(3), Rh1–P2 2.283(3), Rh1–I1 2.591(1). Selected bond angles for **3c** (°): N1–Rh1–P1 84.9(3), N1–Rh1–P2 85.3(3), P1–Rh1–P2 167.0(1), N1–Rh1–I1 173.7(2), P1–Rh1–I1 94.27(7), P2–Rh1–I1 94.62(8).

While attempting to generate (^{Mes}PNP)Rh(Me)(I)$_2$ (**3d**) through oxidative addition of MeI to (^{Mes}PNP)RhI (**3c**), the product of intramolecular mesityl methyl C–H activation, (^{Mes}PNP*)Rh(I)$_2$ (**3d"**), was obtained (Scheme 11). The structure of **3d"** was determined by X-ray crystallography (Figure 10). ^{31}P{^{1}H} NMR spectrum of **3d"** shows a two-bond P-P coupling constant of 462 Hz, which is within the range of common $^2J_{PP}$ between two *trans* phosphorus atoms.[89,90] Similar C–H activations of the methyl of mesityl or mesitylene by late transition metal complexes has been reported.[11,91-95] The oxidative addition product, (^{Mes}PNP)Rh(Me)(I)$_2$ (**3d**), could be observed by NMR spectroscopy, but attempts to isolate it were not successful due to the conversion to **3d"** and methane. The ^{1}H NMR spectrum of the reaction between **3c** and MeI reveals a triplet of doublets at 1.59 ppm assigned to the Rh–CH_3 of (^{Mes}PNP)Rh(Me)(I)$_2$ (**3d**). This resonance is absent when **3c** is reacted with CD_3I. Also, the ^{1}H NMR spectrum of (^{Mes}PNP)Rh(Me)(I)$_2$ (**3d**) is consistent with the loss of a mirror plane after reacting with MeI, compared to **3c**. A doublet with a $^1J_{PRh}$ of 106 Hz was observed in the ^{31}P{^{1}H} NMR spectrum. Methane (0.19 ppm, singlet) was observed as a product along with the formation of **3d"**, and, for the reaction of

3c with CD_3I, the observed septet at 0.14 ppm the ^1H NMR spectrum is assigned to CD_3H (Figure 9). It is notable that in the reaction of **3a** and MeI, methane release was also observed, which suggests the formation of a similar product, (^{Mes}PNP*)Rh(Cl)(I) (**3b"**).

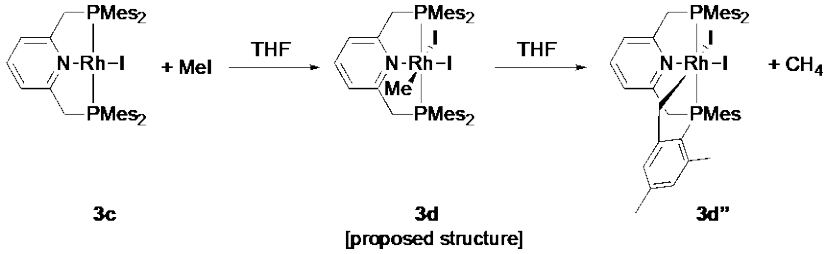

Scheme 11. C–H activation of the mesityl substituent of (^{Mes}PNP)RhI (**3c**) in THF.

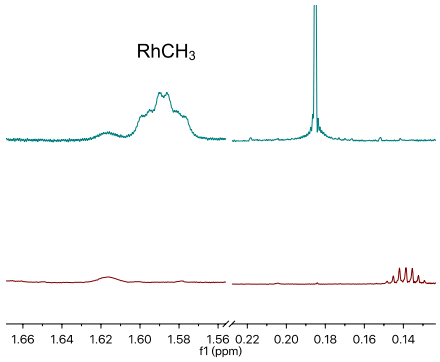

Figure 9. Top: Peaks assigned to Rh–CH_3 (left) and CH_4 (right) in the ^1H NMR spectrum of the reaction **3c** with CH_3I. Bottom: ^1H NMR spectrum of the reaction of **3c** with CD_3I. Reactions were performed in THF-d_8 at room temperature.

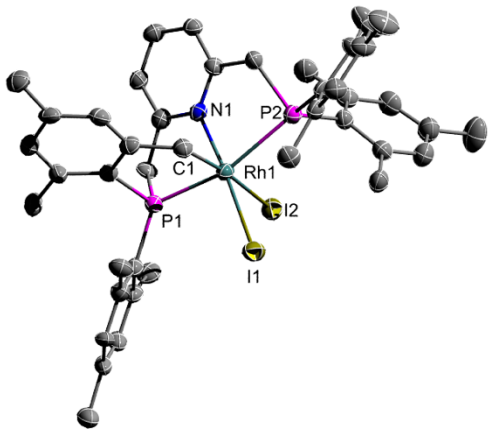

Figure 10. ORTEP of (^{Mes}PNP*)Rh$(I)_2$ (**3d"**). Ellipsoids are drawn at 50% probability level and hydrogen

atoms are omitted for clarity. Selected bond lengths for **3d"** (Å): Rh1–N1 2.093(5), Rh1–C1 2.105(7), Rh1–P1 2.262(2), Rh1–P2 2.481(2), Rh1–I1 2.6622(7), Rh1–I2 2.8175(8). Selected bond angles for **3d"** (°): N1–Rh1–C1 87.0(2), N1–Rh1–P1 81.3(2), C1–Rh1–P1 82.6(2), N1–Rh1–P2 81.8 (2), C1–Rh1–P2 94.1(2), P1–Rh1–P2 162.92(6), N1–Rh1–I1 175.7(2), C1–Rh1–I1 92.4(2), P1–Rh1–I1 94.45(5), P2–Rh1–I1 102.45(4), N1–Rh1–I2 92.5(2), C1–Rh1–I2 173.1(2), P1–Rh1–I2 90.53(5), P2–Rh1–I2 92.68(5), I1–Rh1–I2 87.59(2), C3–P1–C10 107.1(3).

Reactions of (^{Ph}PNP)RhCl (4a). (^{Ph}PNP)RhCl (**4a**) was synthesized by stirring a THF solution of $[Rh(\mu\text{-}C_2H_4)_2Cl]_2$ with ^{Ph}PNP (2 equivalents).[82,96] The equivalency of four phenyl groups and four PCH_2 protons in the ^{1}H NMR spectrum of (^{Ph}PNP)RhCl (**4a**) is consistent with the formation of **4a**, and the $^1J_{PRh}$ of 150 Hz of **4a** is consistent with a Rh^I oxidation state. Adding MeI to a benzene solution of (^{Ph}PNP)RhCl (**4a**) gives two Rh^{III} products (Scheme 12). The major product (**4b-1**) is one isomer of (^{Ph}PNP)Rh(Me)(Cl)(I), with methyl and iodide *trans* to each other, which is confirmed by X-ray crystallography (Figure 11). The another product is assigned as another isomer of (^{Ph}PNP)Rh(Me)(Cl)(I), but efforts to confirm the structure by X-ray diffraction were not successful. Similar as **2b,** heating a THF-d_8 suspension of **4b** at 90 °C did not give the corresponding reductive elimination product.

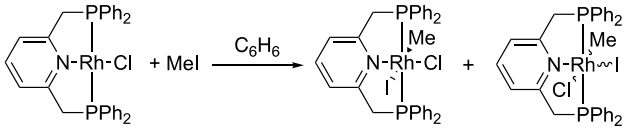

4a **4b-1**

Scheme 12. Oxidative addition of MeI to (^{Ph}PNP)RhCl (**4a**) in benzene.

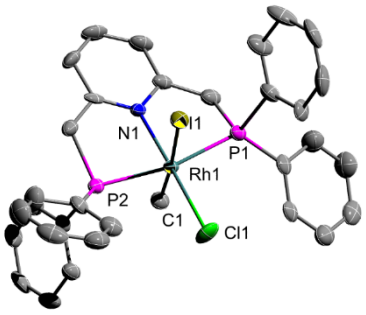

Figure 11. ORTEP of (^{Ph}PNP)Rh(Me)(Cl)(I) (isomer **4b-1**). Ellipsoids are drawn at 50% probability level

and hydrogen atoms are omitted for clarity. Selected bond lengths for **4b-1** (Å): Rh1–N1 2.059(6), Rh1–C1 2.10(2), Rh1–P2 2.298(2), Rh1–P1 2.307(2), Rh1–Cl1 2.359(2), Rh1–I1 2.686(1). Selected bond angles for **4b-1** (°): N1–Rh1–C1 86.1(6), N1–Rh1–P2 82.9(2), C1–Rh1–P2 89.6(5), N1–Rh1–P1 83.9(2), C1–Rh1–P1 89.3(5), P2–Rh1–P1 166.83(8), N1–Rh1–Cl1 178.6(2), C1–Rh1–Cl1 93.6(5), P2–Rh1–Cl1 95.74(9), P1–Rh1–Cl1 97.43(9), N1–Rh1–I1 90.3(2), C1–Rh1–I1 175.7(5), P2–Rh1–I1 87.77(7), P1–Rh1–I1 92.45(7), Cl1–Rh1–I1 90.00(7).

Oxidative addition of CH_2Cl_2 to (^{R}PNP)RhCl. CH_2Cl_2 was added to solutions of the four (^{R}PNP)RhCl complexes in order to compare oxidative addition reactions to form (^{R}PNP)Rh(CH_2Cl)$(Cl)_2$. The oxidative addition of CH_2Cl_2 only occurred with smaller substituents on phosphorus (i.e., for R = ^{i}Pr and Ph). In the reaction of (^{iPr}PNP)RhCl (**2a**), two isomers, *cis*-(^{iPr}PNP)Rh(CH_2Cl)Cl_2 (**2e-*cis***) and *trans*-(^{iPr}PNP)Rh(CH_2Cl)Cl_2 (**2e-*trans***), were formed in a 2:1 ratio, according to the integration of 3,5-H of pyridyl in the ^{1}H NMR spectrum (Scheme 13 and Figure 12). The structures of **2e-*cis*** and **2e-*trans*** have been confirmed by a single crystal X-ray diffraction study (Figure 13). In the reaction of (^{Ph}PNP)RhCl (**4a**), only *cis*-(^{Ph}PNP)Rh(CH_2Cl)Cl_2 (**4e-*cis***) was observed by ^{1}H NMR spectroscopy, and the structure was confirmed by single crystal X-ray diffraction study (Figure 13). There is no reaction between CH_2Cl_2 and (^{R}PNP)RhCl when R = ^{t}Bu, Mes. We attempted to gain evidence for the reversible reductive elimination of CH_2Cl_2 from complexes **2e** (a mixture of **2e-*cis*** and **2e-*trans***) and **4e-*cis*** by heating solutions of the Rh^{III} complexes in CD_2Cl_2. Reversible reductive elimination should produce free CH_2Cl_2 and Rh–CD_2Cl complexes; however, no reductive elimination was observed, indicating that the oxidative addition products are likely highly favored for these Rh^{III} complexes.

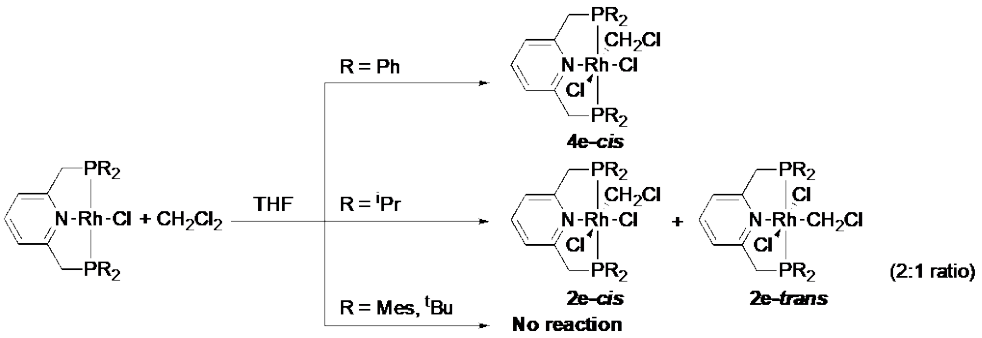

Scheme 13. Attempted oxidative addition reactions of CH_2Cl_2 with the Rh complexes (^{R}PNP)RhCl (R = ^{t}Bu, ^{i}Pr, Mes, Ph).

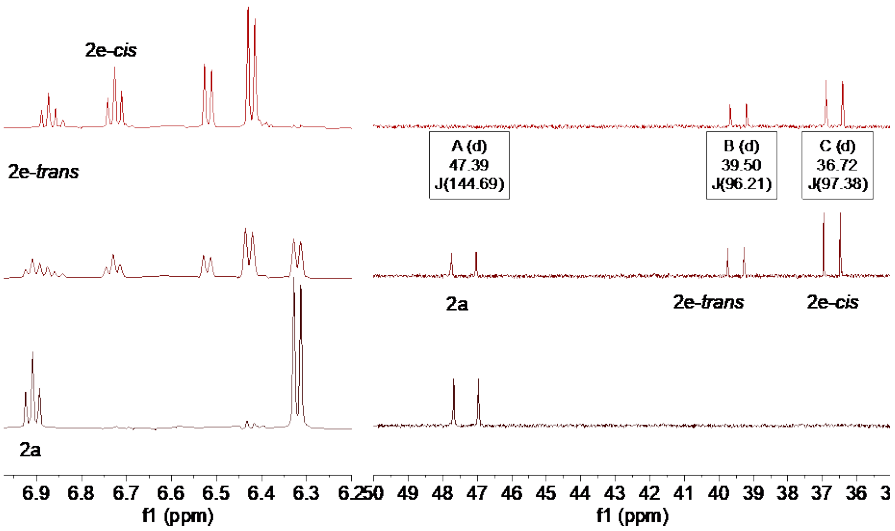

Figure 12. ^{1}H NMR (pyridyl region, left) and ^{31}P{^{1}H} NMR (right) spectra from the reaction of (^{iPr}PNP)RhCl (**2a**) and CH_2Cl_2 to form *cis*-(^{iPr}PNP)Rh(CH_2Cl)Cl_2 (**2e-*cis***, 36.7 ppm, $^{1}J_{PRh}$ = 97 Hz in ^{31}P{^{1}H} NMR) and *trans*-(^{iPr}PNP)Rh(CH_2Cl)Cl_2 (**2e-*trans***, 39.5 ppm, $^{1}J_{PRh}$ = 96 Hz in ^{31}P{^{1}H} NMR). From bottom to top: starting complex **2a**, reaction after 4 hours and after 15 hours. Reaction conditions: 60 °C, C_6D_6 as the solvent.

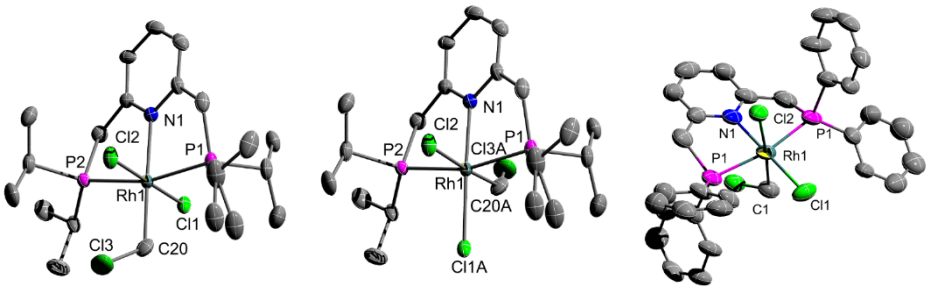

Figure 13. ORTEPs of (^{iPr}PNP)Rh(CH_2Cl)Cl_2 (**2e**; **2e-*cis*** on the left and **2e-*trans*** in the middle) and *cis*-(^{Ph}PNP)Rh(CH_2Cl)Cl_2 (**4e-*cis***, right). Ellipsoids are drawn at 50% probability level and hydrogen atoms are omitted for clarity. **2e** refers to the mixture of **2e-*cis*** and **2e-*trans***. Selected bond lengths for **2e** (Å): Rh1–N1 2.143(3), Rh1–P1 2.3434(9), Rh1–P2 2.3472(9), Rh1–Cl2 2.3669(8). Selected bond lengths for **2e-*cis*** (Å): Rh1–C20A 2.08(8), Rh1–Cl1A 2.41(2). Selected bond lengths for **2e-*trans*** (Å): Rh1–C20 2.099(5), Rh1–Cl1 2.365(1). Selected bond angles for **2e** (°): N1–Rh1–P1 81.96(7), N1–Rh1–P2 82.02(7), P1–Rh1–P2 163.95(3), P1–Rh1–Cl2 84.35(3). Selected bond angles for **2e-*cis*** (°): C20A–Rh1–N1 87.0(3), C20A–Rh1–P1 94.(3), C20A–Rh1–P2 86.(3), C20A–Rh1–Cl2 176.(3), N1–Rh1–Cl2 89.29(7), P2–Rh1–Cl2 94.52(3), C20A–Rh1–Cl1A 85.(3), N1–Rh1–Cl1A 171.3(4), P1–Rh1–Cl1A 100.9(4), P2–Rh1–Cl1A 95.1(4), Cl2–Rh1–Cl1A 99.1(4). Selected bond angles for **2e-*trans*** (°): C20–Rh1–N1 177.9(2), C20–Rh1–P1 97.4(2), N1–C20–Rh1–P2 98.6(2), C20–Rh1–Cl1 87.5(1), N1–Rh1–Cl1 90.53(7), P1–Rh1–Cl1 95.13(4), P2–Rh1–Cl1 85.95(4), C20–Rh1–Cl2 92.7(1), N1–Rh1–Cl2 89.29(7), P2–Rh1–Cl2 94.52(3), Cl1–Rh1–Cl2 179.47(4). Selected bond lengths for **4e-*cis*** (Å): Rh1–N1 2.081(13), Rh1–C1 2.13(2), Rh1–P1 2.311(3), Rh1–Cl1 2.346(4), Rh1–Cl2 2.536(5). Selected bond angles for **4e-*cis*** (°): N1–Rh1–C1 92.6(8), N1–Rh1–P1 83.31(7), C1–Rh1–P1 90.5(9), C1–Rh1–P1 90.1(9), P1–Rh1–P1 166.61(14), N1–Rh1–Cl1 180.0, C1–Rh1–Cl1 87.4(8), P1–Rh1–Cl1 96.69(7), N1–

Rh1–Cl2 89.0(2), P1–Rh1–Cl2 95.8(2), P1–Rh1–Cl2 84.0(2), Cl1–Rh1–Cl2 91.0(2), N1–Rh1–Cl2 89.0(2), P1–Rh1–Cl2 84.0(2), P1–Rh–Cl2 95.8(2), Cl1–Rh1–Cl2 91.0(2), Cl2–Rh1–Cl2 178.0(3).

Activation and reaction free energies were calculated for the S_N2 addition of CH_2Cl_2 to the four (^{R}PNP)RhCl complexes (Scheme 14). As for the addition of CH_3I to (^{R}PNP)RhCl, the phosphine substituent exerts a far greater influence on the calculated exothermicity of the reaction than on the activation barrier. The $\Delta G^{\ddagger}$ for R = Mes is 19.3 kcal·mol^{-1}, 5 kcal·mol^{-1} higher than the phenyl analog. For R = ^{t}Bu, $\Delta G^{\ddagger}$ = 18.8 kcal·mol^{-1}, only two kcal·mol^{-1} higher than for R = ^{i}Pr. This small difference may not explain the distinct reactivity observed for the two alkyl substituents. The standard reaction free energies for the bulky substituents R = ^{t}Bu and Mes are +2.0 kcal·mol^{-1} and –8.5 kcal·mol^{-1}, respectively, while the reactions with R = ^{i}Pr and Ph are irreversibly exergonic at ΔG = −26.7 kcal·mol^{-1} and –25.6 kcal·mol^{-1}. Again, the stability of the Rh^{III} intermediates is consistent with the absence of elimination reactions for the smaller substituents.

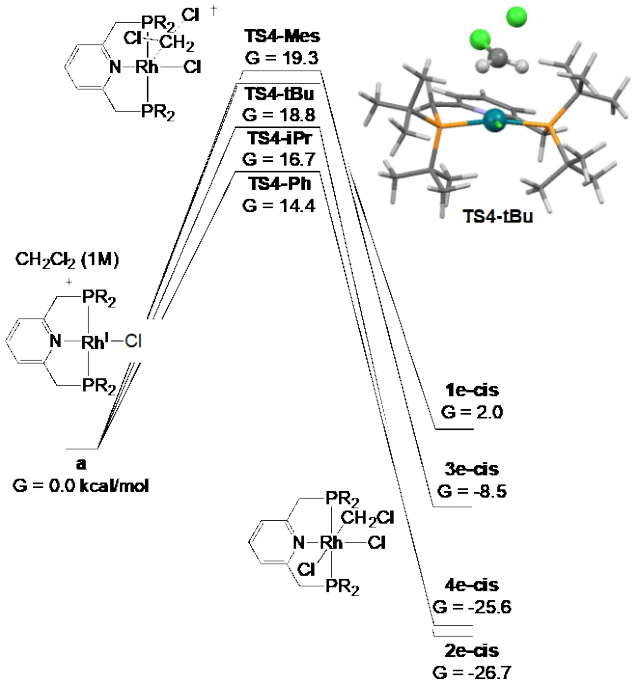

Scheme 14. Computed activation and reaction free energies (kcal·mol^{-1} at 298 K in THF) for the addition of CH_2Cl_2 to (^{R}PNP)Rh^{I}Cl complexes.

CONCLUSIONS

We speculated that axial steric bulk of PNP ligands could be used to control the energetics of Rh$^{I/III}$

oxidative addition/reductive elimination sequences. The hypothesis was validated by combining computational modeling and experimental studies (Scheme 13). For reactions of MeI with (^{R}PNP)RhCl complexes, the results vary with the identity of the substituents R. For the large substituents such as *tert*-butyl and mesityl, MeI oxidative addition is slow relative to PNP ligands with the smaller substituents, and subsequent MeCl reductive elimination is observed. In contrast, the smaller substituents *iso*-propyl and phenyl facilitate MeI oxidative addition, and the reductive elimination of MeCl or MeI was not observed due to the high stability of Rh^{III} products. While the results are consistent with steric influence being most important, it is not possible to eliminate a potential role for ligand donor ability as a function of the substituents. When using CH_2Cl_2 as the oxidative addition reagent, the reactions only occur with PNP ligands that possess the smaller substituents, *iso*-propyl and phenyl. An Eyring analysis for the oxidative addition of MeI to (^{tBu}PNP)RhCl (**1a**) indicates that the $\Delta H^{‡}$ and $\Delta S^{‡}$ are 10.4(8) kcal·mol^{-1} and −34(2) cal·mol^{-1}·K^{-1}, respectively. The $\Delta G^{‡}$ at −78 °C is ~17 kcal·mol^{-1}. The rate of oxidative addition of MeI to (^{iPr}PNP)RhCl (**2a**) at −78 °C is too fast to be measured by NMR spectroscopy, but an upper limit for the $\Delta G^{‡}$ of ≤ 13 kcal·mol^{-1} was estimated. Thus, the $\Delta\Delta G^{‡}$ for MeI oxidative addition to **1a** and **2a** is proposed to be ≥ 4 kcal·mol^{-1}. Calculated thermochemistry corroborates that the activation barriers for S_N2 addition reactions at square planar Rh^{I}, which require access to only one site, are perturbed by 2-5 kcal·mol^{-1} when steric bulk is varied. The stability of six-coordinate products, however, changes by more than 25 kcal·mol^{-1}. These results indicate that the rates of $Rh^{I/III}$ oxidative addition/reductive elimination processes can be controlled through variation of axial steric bulk (Scheme 15). By adjusting the steric properties of the intermediates in the proposed mechanism of hydrocarbon oxidations (Scheme 1), it offers another stragety to tune the energetics of both C–H activation and reductive

elimination.

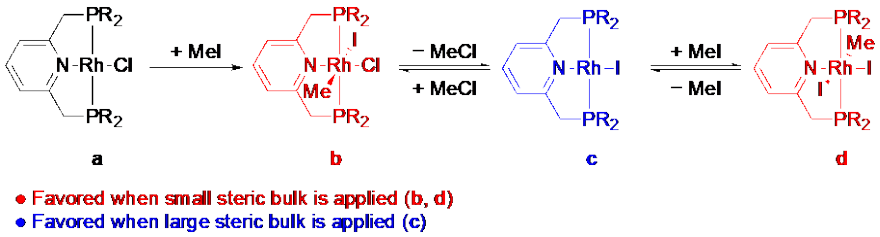

Scheme 15. Axial steric effect on the oxidative addition and reductive elimination of (^{R}PNP)Rh complexes.

EXPERIMENTAL SECTION

General Methods. Unless otherwise noted, all reactions and manipulations were performed under a nitrogen atmosphere in a glovebox or using standard Schlenk techniques with dried and degassed solvents. All solvents were reagent grade or better. Deuterated solvents were used as received. All the solvents were kept in the glovebox over 4 Å molecular sieves. All NMR spectra were recorded on Varian Inova 600 MHz or 500 MHz spectrometer, or Bruker Avance III 800 MHz spectrometer. Operating frequency for $^{13}C\{^{1}H\}$ NMR is 150 MHz (on 600 MHz instrument) or 201 MHz (on 800 MHz instrument), and for $^{31}P\{^{1}H\}$ NMR is 243 MHz (on 600 MHz instrument) or 202 MHz (on 500 MHz instrument). All ^{1}H and $^{13}C\{^{1}H\}$ NMR spectra are referenced against residual ^{1}H resonances (^{1}H NMR) or $^{13}C\{^{1}H\}$ resonances ($^{13}C\{^{1}H\}$ NMR) of the deuterated solvents. $^{31}P\{^{1}H\}$ NMR spectra are referenced with 85% H_3PO_4 in H_2O (used as an external standard). All spectra were recorded at 25 °C unless otherwise indicated. For the variable temperature NMR experiments, the temperature is calibrated using methanol.[97] Literature procedures were used to prepare ^{tBu}PNP, ^{iPr}PNP, ^{Mes}PNP, ^{Ph}PNP and $[Rh(C_2H_4)_2Cl]_2$.[89,96,98-100]

Synthesis and Characterization. (^{tBu}PNP)RhCl (1a). A procedure modified from literature is applied.[83] In a glass vial a THF (5 mL) solution of ^{tBu}PNP (210 mg, 531 μmol) was added to a THF (5 mL) solution of $[Rh(\mu\text{-}C_2H_4)_2Cl]_2$ (110 mg, 283 μmol) and stirred for 10 min. The color turned from orange to red. The solvent was removed under vacuum, and the solid was washed with pentane (5 mL × 2) and then dried under vacuum, and the pure product of (^{tBu}PNP)RhCl was obtained as a red solid. The isolated yield is 81%. ^{1}H NMR (C_6D_6, 600 MHz): δ 6.89 (t, 1H, $^3J_{HH}$ = 8 Hz, py H-4), 6.27 (d, 2H, $^3J_{HH}$ = 8 Hz, py H-3,5), 2.57 (vt, 4H, C*H*$_2$P), 1.46 (vt, 36H, $^2J_{HP}$ = 6 Hz, PC(C*H*$_3$)$_3$). ^{13}C{^{1}H} NMR (C_6D_6, 151 MHz): δ 164.4 (vt, py C-2,6), 128.7 (s, py C-4), 119.8 (vt, $^3J_{PC}$ = 5 Hz, py C-3,5), 36.5 (vt, *C*H$_2$P), 34.9 (vt, P*C*(CH$_3$)$_3$), 29.6 (vt, PC(*C*H$_3$)$_3$). ^{31}P{^{1}H} NMR (C_6D_6, 243 MHz): δ 58.1 (d, $^1J_{PRh}$ = 145 Hz).

(^{iPr}PNP)RhCl (2a). A procedure modified from the literature was used.[45] A THF solution (3 mL) of ^{iPr}PNP (95.6 mg, 282 μmol) was added to a stirred solution of $[Rh(\mu\text{-}C_2H_4)_2Cl]_2$ (54.8 mg, 141 μmol) in THF (5 mL) leading to a color change from orange to dark red. The reaction mixture was stirred at ambient temperature for 30 min followed by solvent removal under vacuum to give a red solid. The solid was washed with cold pentane (5 mL × 2). The isolated yield is 72%. Crystals suitable for X-ray analysis were obtained by layering a concentrated THF solution of (^{iPr}PNP)RhCl with pentane. ^{1}H NMR (C_6D_6, 600 MHz): δ 6.90 (t, $^3J_{HH}$ = 8 Hz, 1H, py 4-H), 6.30 (d, $^3J_{HH}$ = 8 Hz, 2H, py 3,5-H), 2.44 (vt, $^2J_{PH}$ = 4 Hz, 4H, PC*H*$_2$), 2.08 (svt, $^3J_{HH}$ = 8 Hz, 4H, C*H*), 1.52 (dvt, 12H, Me of ^{i}Pr), 1.07 (dvt, 12H, Me of ^{i}Pr). ^{13}C{^{1}H}NMR (C_6D_6, 151 MHz): δ 163.9 (vt, py C-2,6), 128.9 (s, py C-4), 112.0 (vt, py C-3,5), 35.9 (vt, *C*H$_2$P), 24.3 (vt, *C*HMe$_2$), 19.4 (vt, CH(*C*H$_3$)$_2$), 18.0 (s, vt, CH(*C*H$_3$)$_2$). ^{31}P{^{1}H} NMR (C_6D_6, 243 MHz): δ 47.4 (d, $^1J_{PRh}$ = 145 Hz).

(^{Mes}PNP)RhCl (3a). In a 100 mL round bottom flask, a THF (20 mL) solution of ^{Mes}PNP (31.7 mg,

492 μmol,) was added to a THF (20 mL) solution of $[Rh(\mu\text{-}C_2H_4)_2Cl]_2$ (95.6 mg, 246 μmol,) and stirred for 3 hours. The color turned from orange to red. The solvent was removed under vacuum, and the solid was washed with pentane (10 mL × 2) and then dried under vacuum. The pure product of (^{Mes}PNP)RhCl was obtained as a red solid with 62% yield. Crystals suitable for X-ray analysis were obtained by slowly evaporating pentane into a concentrated THF solution of (^{Mes}PNP)RhCl. ^{1}H NMR (THF-d_8, 600 MHz): δ 7.52 (t, 1H, $^3J_{HH}$ = 8 Hz, py H-4), 7.04 (d, 2H, $^3J_{HH}$ = 8 Hz, py H-3,5), 6.73 (s, 8H, mesityl H-3,5), 4.00 (vt, 4H, PCH_2), 2.19 (s, 12H, mesityl 4-Me), 2.15 (s, 24H, mesityl 2,6-Me). ^{13}C{^{1}H} NMR (DCM-d_2, 151 MHz): 163.6 (vt, py C-2,6), 141.1 (vt, Mes C-2,6), 138.8 (s, Mes C-4), 133.2 (vt, Mes C-1), 130.8 (vt. Mes C-3,5), 128.9 (s, py C-4), 121.1 (vt, py C-3,5), 48.0 (vt, CH$_2$P), 25.2 (vt, Mes 2,6-CH$_3$), 21.1 (s, Mes 4-CH$_3$). ^{31}P{^{1}H} NMR (THF-d$_8$, 243 MHz): δ 11.8 (d, $^1J_{RhP}$ = 143 Hz). Acceptable elemental analysis results for **3a** could not be obtained. The NMR spectra of **3a** appear in Figure S7, S8 and S9.

(^{Ph}PNP)RhCl (4a). A procedure modified from literature was used.[82] In a 100 mL round bottom flask, a THF (20 mL) suspension of ^{Ph}PNP (270 mg, 560 μmol) was added to a THF (5 mL) solution of $[Rh(C_2H_4)_2Cl]_2$ (120 mg, 309 μmol) and stirred for 90 min. The reaction mixture turned to a red suspension. The mixture was filtered, and the precipitate was washed with pentane (5 mL × 2) and dried. The product (^{Ph}PNP)RhCl was isolated as a reddish orange solid in 43% yield. ^{1}H NMR (C_6D_6, 600 MHz): δ 8.17 (8H, m, phenyl H-2,6), 7.06 (t, 8H, $^3J_{HH}$ = 7 Hz, phenyl H-3,5), 7.00 (t, 4H, $^3J_{HH}$ = 7 Hz, phenyl H-4), 6.76 (t, 1H, $^3J_{HH}$ = 8 Hz, py H-4), 6.28 (t, 2H, $^3J_{HH}$ = 8 Hz, py H-3,5), 3.21 (vt, 4H, CH_2P). ^{13}C{^{1}H} NMR (C_6D_6, 151 MHz): δ 162.3 (vt, py C-2,6), 135.7 (vt, Ph C-1), 133.5 (vt, Ph C-2,6), 130.6 (s, Ph C-4), 129.7 (s, py C-4), 128.7 (vt, Ph C-3,5), 120.5 (vt, py C-3,5), 44.0 (vt, CH$_2$P). ^{31}P{^{1}H} NMR (C_6D_6, 243 MHz): δ 22.2 (d, $^1J_{PRh}$ = 150 Hz).

(^{iPr}PNP)Rh(Me)(Cl)(I) (2b). In a glass vial, 0.5 mL of MeI was added dropwise into a stirring THF (10 mL) solution of (^{iPr}PNP)RhCl (54.1 mg, 113 μmol,). The solution turned from red to yellow in 5 seconds. The solvent was removed under vacuum. The product was dissolved in a minimal amount of DCM (3 mL), crushed out with addition of pentane (50 mL) and collected by filtration. The solid was washed with pentane (10 mL × 2) and then dried under vacuum. The product (^{iPr}PNP)Rh(Me)(Cl)(I) was obtained as a yellow solid. The isolated yield is 78%. Crystals suitable for X-ray analysis were obtained by slowly evaporating MeI into a benzene solution of (^{iPr}PNP)RhCl. The NMR is the data for one isomer of **2b-1** and **2b-2**, and the elemental analysis data is for the mixture of two complexes. ^{1}H NMR (C_6D_6, 600 MHz): δ 6.70 (t, $^{3}J_{HH}$ = 8 Hz, 1H, py 4-H), 6.39 (d, $^{3}J_{HH}$ = 8 Hz, 2H, py 3,5-H), 4.05 (m, 2H, C*H*), 3.86 (dvt, $^{2}J_{HH}$ = 17 Hz, 2H, PCH_2), 3.01 (dvt, $^{2}J_{HH}$ = 17 Hz, 2H, PCH_2), 2.45 (m, 2H, C*H*), 1.68 (q, *J* = 8 Hz, 6H, Me of ^{i}Pr), 1.52 (td, $^{2}J_{RhH}$ = 2 Hz, 3H, Rh−Me), 1.33 (q, *J* = 7 Hz, 6H, Me of ^{i}Pr), 1.19 (q, *J* = 7 Hz, 6H, Me of ^{i}Pr), 1.07 (q, 6H, Me of ^{i}Pr). ^{13}C{^{1}H} NMR (THF-d_8, 151 MHz): 163.9 (vt, py C-2,6), 136.0 (s, py C-4), 120.8 (vt, py C-3,5), 40.2 (vt, P*C*H_2), 30.6 (vt, P*C*HMe_2), 23.6 (vt, P*C*HMe_2), 20.1 (s, CH(*C*H_3)$_2$), 19.9 (s, CH(*C*H_3)$_2$), 19.8 (s, CH(*C*H_3)$_2$), 19.4 (s, CH(*C*H_3)$_2$). ^{31}P{^{1}H} NMR (C_6D_6, 243 MHz): δ 36.0 (d, $^{1}J_{PRh}$ = 100 Hz). Anal. Calcd for $C_{20}H_{38}ClINP_2Rh$: C, 38.76; H, 6.18; N, 2.26. Found: C, 38.98; H, 6.33; N, 2.28.

(^{Ph}PNP)Rh(Me)(Cl)(I) (4b-1). In a 20 mL glass vial, (^{Ph}PNP)RhCl (82.9 mg, 135 μmol) was dissolved in 10 mL CH_2Cl_2. The reaction mixture was stirred overnight, and the solvent was evacuated under vacuum. The product was dissolved in a minimal amount of DCM (3 mL), precipitated with addition of pentane (50 mL) and collected by filtration. The product was washed with pentane (10 mL × 2). A yellow solid was obtained as the final product. The isolated yield is 89%. Crystals suitable for X-ray analysis

were obtained by slowly evaporating MeI into a benzene solution of (^{Ph}PNP)RhCl. ^{1}H NMR (600 MHz, DCM-d_2): δ 7.95 (m, 4H, phenyl *H*), 7.74 (t, 1H, $^{3}J_{HH}$ = 8 Hz, py *H*-4), 7.68 (m, 4H, phenyl *H*), 7.52 (d, 2H, $^{3}J_{HH}$ = 8 Hz, py *H*-3,5), 7.41 (m, 12H, phenyl *H*), 4.80 (vdt, 2H, $^{3}J_{RhH}$ = 5 Hz, PCH_2), 4.39 (vdt, 2H, $^{3}J_{RhH}$ = 5 Hz, PCH_2), 0.72 (td, 3H, $^{1}J_{RhH}$ = 2 Hz, $^{2}J_{PH}$ = 6 Hz, Rh–CH_3). ^{13}C{^{1}H} NMR (202 MHz, DCM-d_2): 163.1 (vt), 138.6, 134.8 (vt), 132.8 (vt), 131.4, 130.9, 129.1 (vt), 128.5 (vt), 122.3 (vt), 42.9 (vt). ^{31}P{^{1}H} NMR (243 MHz, DCM-d_2): δ 23.2 (d, $^{1}J_{PRh}$ = 106 Hz). Anal. Calcd for $C_{32}H_{30}ClINP_2Rh$: C, 50.85; H, 4.00; N, 1.85. Found: C, 50.82; H, 3.91; N, 1.91.

(^{tBu}PNP)RhI (1c). In a 50 mL round bottom flask, 5 mL of MeI was added to a THF (20 mL) solution of (^{tBu}PNP)RhCl (92.3 mg, 0.172 μmol). The reaction mixture turned from a dark red solution to an orange suspension in 20 seconds. After stirring for 20 min, the solvent was removed under vacuum, and another 20 mL of THF was added. The resulting red solution was again left under vacuum to remove the solvent. The addition of THF and removal of solvent was repeated three times, resulting in dark red solid as the product. The isolated yield is 99%. Crystals suitable for X-ray analysis were obtained by layering a concentrated THF solution of (^{tBu}PNP)RhI with pentane. ^{1}H NMR (CD_2Cl_2, 600 MHz): δ 7.55 (t, 1H, $^{3}J_{HH}$ = 8 Hz, py H-4), 7.04 (d, 2H, $^{3}J_{HH}$ = 8 Hz, py H-3,5), 3.07 (vt, 4H, CH_2P), 1.43 (vt, 36H, PC(CH_3)$_3$). ^{13}C{^{1}H} NMR (C_6D_6, 151 MHz): δ 164.0 (vt, py C-2,6), 130.0 (s, py C-4), 119.7 (vt, $^{3}J_{PC}$ = 5 Hz, py C-3,5), 37.7 (vt, $^{1}J_{PC}$ = 5 Hz, *C*H_2P), 35.4 (vt, $^{1}J_{PC}$ = 6 Hz, P*C*(CH$_3$)$_3$), 30.0 (vt, $^{2}J_{PC}$ = 4 Hz, PC(*C*H$_3$)$_3$). ^{31}P{^{1}H} NMR (CD_2Cl_2, 243 MHz): δ 60.5 (d, $^{1}J_{PRh}$ = 138 Hz).

(^{iPr}PNP)RhI (2c). A reported procedure was used.[87] In a glass vial, an acetone (0.6 mL) solution of NaI (45.5 mg, 304 μmol,) was added into an acetone (0.5 mL) solution of (^{iPr}PNP)RhCl (72.7 mg, 152 μmol,). The reaction mixture was stirred for 10 minutes, and the solvent was removed under vacuum. A

few drops of benzene were added to fully dissolve the red product, and the mixture was filtered through a fine porosity frit loaded with Celite. Benzene was removed under vacuum, and the product was washed with cold pentane (10 mL × 2). A red solid was obtained in 85% yield. ^{1}H NMR (600 MHz, C_6D_6): δ 6.98 (t, $^{3}J_{HH}$ = 8 Hz, 1H, py H-4), 6.38 (d, $^{3}J_{HH}$ = 8 Hz, 2H, py H-3,5), 2.48 (vt, 4H, PCH_2), 2.19 (m, 4H, PCH(CH_3)$_2$), 1.53 (dvt, $^{3}J_{HH}$ = 7 Hz, 12H, PCH(CH_3)$_2$), 0.97 (dvt, $^{3}J_{HH}$ = 7 Hz, 12H, PCH(CH_3)$_2$). ^{13}C{^{1}H} NMR (151 MHz, C_6D_6): δ 163.7 (vt, py C-2,6), 130.0 (s, py C-4), 120.1 (vt, py C-3,5), 36.9 (vt, PCH$_2$), 24.6 (vt, PCH(CH_3)$_2$), 19.8 (br s, PCH(CH$_3$)$_2$), 18.0 (br s, PCH(CH$_3$)$_2$). ^{31}P{^{1}H} NMR (243 MHz, C_6D_6): δ 51.1 (d, $^{1}J_{PRh}$ = 138 Hz). Anal. Calcd for $C_{19}H_{35}INP_2Rh$: C, 40.09; H, 6.20; N, 2.46. Found: C, 39.93; H, 6.17; N, 2.54.

(^{Mes}PNP)RhI (3c). In a glass vial, an acetone solution (3 mL) of NaI (24.6 mg) was added into an acetone suspension (5 mL) of (^{Mes}PNP)RhCl (64.2 mg). The reaction mixture was stirred for 30 min, and it quickly turned from an orange suspension into a dark red solution. After the solvent was removed under vacuum, the mixture was dissolved in 5 mL of benzene, and was filtered through frits loaded with Celite to remove NaCl. Benzene was removed under vacuum, and the product was washed using pentane (5 mL × 2). A dark red solid was obtained as the product after dried under vacuum. The yield is 89%. Crystals suitable for X-ray analysis were obtained by vapor diffusion of pentane into a concentrated THF solution of (^{Mes}PNP)RhI. ^{1}H NMR (C_6D_6, 600 MHz): δ 6.72 (m, 9H, py H-4 and mesityl H), 6.16 (d, 2H, $^{3}J_{HH}$ = 7 Hz, py H-3,5), 3.90 (vt, 4H, PCH_2), 2.80 (s, 24H, mesityl 2,6-Me), 2.05 (s, 12H, mesityl 4-Me). ^{13}C{^{1}H} NMR (C_6D_6, 151 MHz): 162.3 (vt, py C-2,6), 141.1 (vt, Mes C-2,6), 138.4 (s, Mes C-4), 133.4 (vt, Mes C-1), 130.9 (vt. Mes C-3,5), 128.4 (s, py C-4), 120.3 (vt, py C-3,5), 50.1 (vt, CH$_2$P), 26.4 (vt, Mes 2,6-CH$_3$), 20.9 (s, Mes 4-CH$_3$). ^{31}P{^{1}H} NMR (C_6D_6, 243 MHz): δ 14.2 (d, $^{1}J_{RhP}$ = 140 Hz).

Acceptable elemental analysis results for **3c** could not be obtained. The NMR spectra of **3c** appear in Figure S25, S26 and S27.

[(^{tBu}PNP)Rh(Me)I]I (1d'). In a 50 mL round bottom flask, 5 mL MeI were added to a THF (20 mL) solution of (^{tBu}PNP)RhCl (92.3 mg, 172 μmol,). The reaction mixture turned from a dark red solution to a orange suspension in 20 seconds. The reaction mixture was allowed to stir overnight. The mixture was filtered, and the solid was washed with a mixture of MeI and pentane (1:3 v/v, 10 mL) and dried under vacuum. The product was obtained as an orange solid, and the NMR spectra are consistent with published results.[44] The yield is 65%. ^{1}H NMR (600 MHz, DCM-d_2): δ 8.01-7.93 (m, 3H, py H-3,4,5), 4.30 (dvt, $^{2}J_{HH}$ = 18 Hz, 2H, PCH_2), 4.04 (dvt, $^{2}J_{HH}$ = 18 Hz, 2H, PCH_2), 2.30 (vtd, $^{2}J_{RhH}$ = 3 Hz, 3H, RhCH_3), 1.56 (vt, 18H, PC(CH_3)$_3$), 1.38 (vt, 18H, PC(CH_3)$_3$). ^{13}C{^{1}H} NMR (DCM-d_2, 151 MHz): 165.1 (vt, py C-2,6), 140.1 (s, py C-4), 124.1 (vt, py C-3,5), 39.2 (vtd, $^{2}J_{RhC}$ = 2 Hz, PCH$_2$), 38.1 (vt, PC(CH$_3$)$_3$), 37.5 (vt, PC(CH$_3$)$_3$), 31.3 (vt, PC(CH$_3$)$_3$), 29.8 (vt, PC(CH$_3$)$_3$), 9.2 (dt, $^{1}J_{RhC}$ = 25 Hz, $^{2}J_{PC}$ = 4 Hz, RhCH$_3$). ^{31}P{^{1}H} NMR (243 MHz, DCM-d_2): δ 51.8 (d, $^{1}J_{PRh}$ = 100 Hz). Leaving the sample under vacuum for 2 weeks did not remove all the THF, and 0.08 molecule of THF is included in calculation of theoretical value of elemental analysis, based on the integration in ^{1}H NMR spectrum. Calcd for $C_{24.32}H_{46.64}I_2NP_2RhO_{0.08}$: C, 37.78; H, 6.08; N, 1.81. Found: C, 38.03; H, 6.25; N, 1.87.

***cis*-(^{iPr}PNP)Rh(Me)(I)$_2$ (2d).** The procedure was modified from literature.[45] In a 100 mL round bottom flask, (^{iPr}PNP)RhI (54.2 mg, 95 μmol) was dissolved in THF, and 0.5 mL of MeI was added. The solution quickly turned from red to bright yellow. The reaction mixture was stirred for 10 min, and then the solvent was removed under vacuum. The resulting solid was dissolved in small amount of DCM, and 50 mL of pentane was added to precipitate the product. The mixture was filtered through a frit with fine

porosity, and the yellow solid, *cis*-(^{iPr}PNP)Rh(Me)I_2, was collected. The product was washed with pentane (5 mL × 2). The isolated yield is 88%. ^{1}H NMR (C_6D_6, 600 MHz): δ 6.69 (t, $^3J_{HH}$ = 8 Hz, 1H, py 4-H), 6.38 (d, $^3J_{HH}$ = 8 Hz, 2H, py 3,5-H), 3.97-3.90 (m, 4H, C*H* and PCH_2), 3.08 (dvt, $^2J_{HH}$ = 17 Hz, 2H, PCH_2), 2.47 (m, 2H, C*H*), 1.71 (q, *J* = 8 Hz, 6H, Me of ^{i}Pr), 1.40 (td, $^2J_{RhH}$ = 2 Hz, 3H, Rh−Me), 1.37 (q, *J* = 7 Hz, 6H, Me of ^{i}Pr), 1.22 (q, *J* = 7 Hz, 6H, Me of ^{i}Pr), 1.06 (q, 6H, Me of ^{i}Pr). ^{13}C{^{1}H} NMR (DCM-d_2, 151 MHz): δ 163.6 (vt, py C-2,6), 137.9 (s, py C-4), 121.7 (vt, py C-3,5), 41.6 (vt, P*C*H_2), 31.0 (vt, *C*H(CH_3)$_2$), 24.6 (vt, *C*H(CH_3)$_2$), 21.5 (s, CH(*C*H_3)$_2$), 21.1 (s, CH(*C*H_3)$_2$), 20.3 (s, CH(*C*H_3)$_2$), 20.1 (s, CH(*C*H_3)$_2$), -0.5 (m, Rh–CH_3). ^{31}P{^{1}H} NMR (C_6D_6, 243 MHz): δ 38.0 (d, $^1J_{PRh}$ = 99 Hz). Calcd for $C_{20}H_{38}I_2NP_2Rh$: C, 33.78; H, 5.39; N, 1.97. Found: C, 34.32; H, 5.55; N, 2.06.

(^{Mes}PNP*)RhI_2 (3d"). In a glass vial, MeI (1 mL) was added dropwise into a THF solution of (^{Mes}PNP)RhI (34.2 mg, 39 μmol). The solution turned from red to yellow quickly. The reaction was allowed to stir for 24 h, and then the solvent was removed under vacuum, and pentane was used to wash the solid. ^{1}H NMR (CD_2Cl_2, 500 MHz): δ 7.41 (t, $^3J_{HH}$ = 7 Hz, 1H, py H-4), 7.16 (d, $^3J_{HH}$ = 8 Hz, 1H, py H-3/5), 7.06 (s, 1H, Mes H-3/5), 7.03 (s, 1H, Mes H), 7.00 (d, $^3J_{HH}$ = 7 Hz, 1H, py H-5/3), 6.88 (s, 1H, Mes H), 6.84 (s, 1H, Mes H), 6.79 (s, 1H, Mes H), 6.66 (s, 2H, Mes H), 6.61 (s, 1H, Mes H), 6.04 (d, $^2J_{HH}$ = 13 Hz, 1H, RhCH_2), 4.85 (d, $^2J_{HH}$ = 15 Hz, 1H, PCH_2), 4.55 (d, $^2J_{HH}$ = 12 Hz, 1H, PCH_2), 4.38 (vtd, $^2J_{HH}$ = 15 Hz, $^2J_{HP}$ = 7 Hz, 1H, RhCH_2), 4.02 (d, $^2J_{HH}$ = 18 Hz, 1H, PCH_2), 3.41 (t, $^2J_{HH}$ = 12 Hz, 1H, PCH_2), 3.19 (s, 3H, Me), 3.16 (s, 3H, Me), 2.33 (s, 3H, Me), 2.31 (s, 3H, Me), 2.29 (s, 3H, Me), 2.24 (s, 3H, Me), 2.09 (s, 3H, Me), 2.06 (s, 3H, Me), 1.94 (s, 3H, Me), 1.91 (s, 3H, Me). ^{13}C{^{1}H} NMR (CD_2Cl_2, 201 MHz): δ 162.4 (s), 160.6 (s), 157.6 (d, $^1J_{CP}$ = 28 Hz), 146.1 (d, $^2J_{CP}$ = 12 Hz), 144.3 (d, $^1J_{CP}$ = 21 Hz), 142.3 (s), 141.7 (s), 141.5 (s), 141.5 (s), 141.3 (s), 141.1 (s), 140.1 (s), 139.1 (d, $^1J_{CP}$ = 27 Hz),

138.2 (s), 133.6 (d, $^{1}J_{CP}$ = 26 Hz), 132.4 (s), 132.3 (s), 131.6 (d, $^{2}J_{CP}$ = 10 Hz), 131.9 (d, $^{2}J_{CP}$ = 8 Hz), 131.8 (d, $^{2}J_{CP}$ = 8 Hz), 129.5 (d, $^{2}J_{CP}$ = 6 Hz), 129.3 (s), 125.9 (s), 125.8 (s), 121.5 (d, $^{3}J_{CP}$ = 12 Hz), 121.2 (d, $^{3}J_{CP}$ = 12 Hz), 53.6 (s, $RhCH_2$), 46.8 (d, $^{1}J_{CP}$ = 19 Hz, PCH_2), 32.8 (d, $^{1}J_{CP}$ = 19 Hz, PCH_2), 26.9 (d, $^{3}J_{CP}$ = 6 Hz), 26.7 (s), 25.4 (s), 24.8 (d, $^{3}J_{CP}$ = 11 Hz), 23.7 (s), 21.3 (s), 21.1 (s), 21.1 (s), 21.0 (s), 20.3 (s). $^{31}P\{^{1}H\}$ NMR (CD_2Cl_2, 243 MHz): δ 61.0 (dd, $^{2}J_{PP}$ = 462 Hz, $^{1}J_{PRh}$ = 113 Hz), 5.8 (dd, $^{2}J_{PP}$ = 462 Hz, $^{1}J_{PRh}$ = 90 Hz). Acceptable elemental analysis results for **3d''** could not be obtained. The NMR spectra of **3d''**, including COSY and HSQC, appear in Figure S34, S35, S36, S37 and S38.

cis*-(^{iPr}PNP)Rh(CH_2Cl)Cl_2 (2e-*cis*) and *trans*-(^{iPr}PNP)Rh(CH_2Cl)Cl_2 (2e-*trans*).** In a 100 mL round bottom flask, (^{iPr}PNP)RhCl (52.6 mg, 110 μmol) was dissolved in DCM (30 mL), and the mixture was stirred for 24 h. The reaction mixture gradually turned from red to light orange. The solvent was removed under vacuum, and the resulting solid was dissolved in minimal amount of DCM (3 mL). 50 mL of pentane was added to precipitate a yellow solid. The product was collected using filtration, washed with pentane (5 mL × 2) and dried under vacuum. The product is a mixture of *cis*-(^{iPr}PNP)Rh(CH_2Cl)Cl_2 and *trans*-(^{iPr}PNP)Rh(CH_2Cl)Cl_2. The isolated yield is 87%. Crystals suitable for X-ray analysis were obtained by vapor diffusion of pentane into a concentrated THF solution of (^{iPr}PNP)Rh(CH_2Cl)Cl_2. *cis*-(^{iPr}PNP)Rh(CH_2Cl)Cl_2 (**2e-*cis). ^{1}H NMR (497 MHz, Benzene-d_6): δ 6.73 (t, $^{3}J_{HH}$ = 8 Hz, 1H, pyridine H-4), 6.42 (d, $^{3}J_{HH}$ = 8 Hz, 2H, pyridine H-3,5), 5.15 (td, $^{3}J_{HP}$ = 7 Hz, $^{2}J_{HRh}$ = 3 Hz, 2H, RhCH_2Cl), 3.67 (dvt, $^{2}J_{HH}$ = 17 Hz, 2H, PCH_2), 3.33 (dvt, $^{2}J_{HH}$ = 17 Hz, 2H, PCH_2), 2.82 (m, 2H, PCHMe$_2$), 2.68 (m, 2H, PCHMe$_2$), 1.66 (dvt, $^{3}J_{HH}$ = 7 Hz, 6H, PCH(CH_3)$_2$), 1.46 (dvt, $^{3}J_{HH}$ = 7 Hz, 6H, PCH(CH_3)$_2$), 1.30 (dvt, $^{3}J_{HH}$ = 7 Hz, 6H, PCH(CH_3)$_2$), 1.06 (dvt, $^{3}J_{HH}$ = 7 Hz, 6H, PCH(CH_3)$_2$). $^{13}C\{^{1}H\}$ NMR (201 MHz, Benzene-d_6): δ 163.8 (vt, pyridine C-2,6), 136.5 (s, pyridine C-4), 120.9 (vt, pyridine C-3,5), 39.2 (vt, PCH_2), 38.19

(dt, $^{1}J_{CRh}$ = 28 Hz, $^{2}J_{CP}$ = 6 Hz, Rh*C*H_2Cl), 24.7 (vt, P*C*HMe_2), 24.2 (vt, P*C*HMe_2), 20.2 (s, PCH(*C*H_3)$_2$), 19.6 (s, PCH(*C*H_3)$_2$), 19.5 (s, PCH(*C*H_3)$_2$), 19.0 (s, PCH(*C*H_3)$_2$). ^{31}P{^{1}H} NMR (201 MHz, Benzene-d_6): 36.7 (d, $^{1}J_{PRh}$ = 97 Hz). *trans*-(^{iPr}PNP)Rh(CH_2Cl)Cl_2 (**2e-*trans***). ^{1}H NMR (497 MHz, Benzene-d_6): δ 6.87 (t, $^{3}J_{HH}$ = 8 Hz, 1H, pyridine H-4), 6.52 (d, $^{3}J_{HH}$ = 8 Hz, 2H, pyridine H-3,5), 5.75 (td, $^{3}J_{HP}$ = 5 Hz, $^{2}J_{HRh}$ = 3 Hz, 2H, RhC*H*$_2$Cl), 3.54 (m, 4H, PC*H*Me_2), 3.49 (vt, 4H, PC*H*$_2$), 1.27 – 1.20 (m, 24H, PCH(C*H*$_3$)$_2$). ^{13}C{^{1}H} NMR (201 MHz, Benzene-d_6): δ 160.9 (vt, pyridine C-2,6), 137.4 (s, pyridine C-4), 120.5 (vt, pyridine C-3,5), 39.1 (vt, P*C*H_2), 34.0 (d, $^{1}J_{CRh}$ = 21 Hz, $^{2}J_{CP}$ = 6 Hz, Rh*C*H_2Cl), 26.0 (vt, P*C*HMe_2), 19.6 (s, PCH(*C*H_3)$_2$), 19.2 (s, PCH(*C*H_3)$_2$). ^{31}P{^{1}H} NMR (201 MHz, Benzene-d_6): 39.5 (d, $^{1}J_{PRh}$ = 96 Hz). Anal. Calcd for $C_{20}H_{37}Cl_3NP_2Rh$: C, 42.69; H, 6.63; N, 2.49. Found: C, 42.85; H, 6.72; N, 2.57.

***cis*-(^{Ph}PNP)Rh(CH_2Cl)Cl_2 (4e-*cis*).** (^{Ph}PNP)RhCl (50 mg, 81.5 μmol) was dissolved in 10 mL DCM, and was allowed to stir for 48 h. The solution gradually turned from red to yellow. The solvent was removed under vacuum, and resulting solid was dissolved in minimal amount of DCM (3 mL). 50 mL of pentane was added into the reaction mixture to precipitate the product. After filtering through a fine porosity frit, the yellow solid, *cis*-(^{Ph}PNP)Rh(CH_2Cl)Cl_2, was washed with 10 mL of pentane and dried under vacuum. The isolated yield is 92%. Crystals suitable for X-ray analysis were obtained by vapor diffusion of DCM into a concentrated benzene solution of (^{Ph}PNP)Rh(CH_2Cl)Cl_2. ^{1}H NMR (600 MHz, CD_2Cl_2): 8.02 (m, 4H, phenyl H), 7.81 – 7.74 (m, 5H, pyridine H-4 and phenyl H), 7.52 (d, $^{3}J_{HH}$ = 8 Hz, 2H, pyridine H-3,5), 7.50 – 7.40 (m, 12H, phenyl H), 4.68 (dvt, $^{2}J_{HH}$ = 17 Hz, 2H, PC*H*$_2$), 4.58 (dvt, $^{2}J_{HH}$ = 17 Hz, 2H, PC*H*$_2$), 3.91 (td, $^{3}J_{HP}$ = 8 Hz, $^{2}J_{HRh}$ = 3 Hz, 2H, RhC*H*$_2$Cl). ^{13}C{^{1}H} NMR (201 MHz, CD_2Cl_2): δ 162.7 (vt), 138.9 (s), 134.6 (vt), 132.6 (vt), 131.3 (s), 131.3 (s), 131.1 (vt), 130.9 (vt), 129.2 (vt), 128.7 (vt), 122.5 (vt), 42.7 (dt, $^{1}J_{CRh}$ = 27 Hz, $^{2}J_{CP}$ = 6 Hz), 42.3 (vt). ^{31}P{^{1}H} NMR (243 MHz, CD_2Cl_2): 27.1 (d,

$^1J_{PRh}$ = 103 Hz). Anal. Calcd for $C_{32}H_{29}Cl_3NP_2Rh$: C, 55.00; H, 4.18; N, 2.00. Found: C, 55.20; H, 4.24; N, 2.10.

Kinetic studies. Oxidative addition of MeI to (^{tBu}PNP)RhCl (1a) in THF-d_8. A J Young NMR tube was charged with a THF-d_8 solution of (^{tBu}PNP)RhCl (**1a**, 16 mM) and hexamethyldisiloxane (HMDSO, internal standard) in the glovebox. After a ^{1}H NMR spectrum was obtained for the starting solution, the J Young tube was brought back into the glove box, and approximately 1 μL of MeI was injected into the tube. The tube was then quickly analyzed and ^{1}H NMR spectra were collected every 1 min using an arrayed experiment. Each data point consists of 4 scans with a delay time of 10 s. Concentrations were determined using the NMR integrals of the 3,5-H of pyridyl of the starting and final complexes. The reactions were run at constant temperature. The reaction was run at 300 K, 309 K, 319 K and 327 K in the NMR instrument with spectra recorded.

Equilibrium between (^{tBu}PNP)RhI (1c) and [(^{tBu}PNP)Rh(Me)I]I (1d') in DCM-d_2. A J Young NMR tube was charged with a DCM-d_2 solution of [(^{tBu}PNP)Rh(Me)I]I (**1d'**, 12 mM) and hexamethylbenzene (HMB, internal standard) in the glovebox. After the ^{1}H NMR was obtained for the starting solution (at this time point there is already an equilibrium established), the J Young tube was brought back into the glove box, and MeI was injected into the tube. Another NMR was taken, and another injection was done. Four points were taken for each sample to calculate the equilibrium constant. The reaction was run at 300 K, 309 K, 319 K and 327 K in the NMR instrument with spectra recorded.

Computational Methods. Species' free enegies (1M at 298K) were calculated as

$$G = G_{sol} + ZPE + H - T(\Delta S_{vib} + \Delta S_{elec} + \Delta S_{trans/rot} - k_B \ln(24.5))$$

including G_{sol} (the sum of the self-consistently determined electronic energy and solvation free energy),

zero point energy, enthalpy and entropy (including vibrational, electronic, translational and rotational contributions as well as the contribution by compression from 1 atm to 1M, which complements the solvation free energy from the continuum model). Geometries were first optimized in vacuum using the B3PW91-D3 functional[101] including the D3 dispersion corrections[102], 6-311G**[103] basis set on organic elements with an extra "tight" *d*-shell (α = 1.35) on phosphorus, 6-311G**++[104] on chlorine, cc-PVTZ-PP[105] sans *f*-functions for iodine, and the Los Alamos small core effective core potential (including 4s and 4p electrons explicitely to better describe shielding of the 4d valence electrons) and triple-ξ valence functions[106] for rhodium. Frequencies computed at these geometries were used for the zero point, enthalpy and entropy terms above. To obtain G_{sol}, geometries were reoptimized with the M06-L[107] functional and we applied PBF implicit solvation[108] (using ε = 7.6 and solvent radius 2.52 Å for THF, ε = 8.55 and solvent radius 2.45 Å for trifluoroacetic acid, ε = 8037 and solvent radius 1.40 Å for water, ε = 8.93 and solvent radius 2.33 Å for DCM, ε = 20.7 and solvent radius 2.44 Å for acetone).

We used a larger basis: 6-311G**++ for organic elements, and 6-311++G-3df-3pd[104] for chlorine and phosphorus. For iodine we used the cc-PVTZ-PP basis set with the Los Alamos effective core potential and we supplemented the valence basis functions with two *f*-shells[109] for rhodium. For the reactions involving CH_2Cl_2 (i.e. Scheme 14), the frequency-dependent terms for all species were calculated using the B3LYP[101,110] functional, 6-31G**++[111,112] basis on non-metal elements, and the Los Alamos effective core potential with double-ζ valence functions. For the survey of anions and ligands in Scheme 5, frequency dependent terms were calculated using B3LYP and 6-31G**. Computed frequencies below 50 cm^{-1} were replaced with a value of 50 cm^{-1} in the calculation of vibrational entropy to avoid spurious contributions to entropy from numerical error in force constants. All calculations were performed with

Jaguar 8.4.[113]

Crystallographic Analysis. A single crystal of **1c**, **2a**, **2b**, **2e**, **3a**, **3c**, **3d''**, **4b-1** or **4e-*cis*** was coated with Paratone oil and mounted on a MiTeGen MicroLoop. The X-ray intensity data were measured on a Bruker Kappa APEXII Duo system. The Incoatec Microfocus IμS (Cu K_α, λ = 1.54178 Å) and a multilayer mirror monochromator were used for **4e-*cis***. The graphite monochromator and a Mo K_α fine-focus sealed tube (λ = 0.71073 Å) were used for all other crystals. All frames were integrated with the Bruker SAINT software package[114] using a narrow-frame algorithm. Data were corrected for absorption effects using the Multi-Scan method (SADABS).[114] Each structure was solved and refined using the Bruker SHELXTL Software Package[115] within APEX3[114] and OLEX2.[116] Non-hydrogen atoms were refined anisotropically. Hydrogen atoms were placed in geometrically calculated positions with U_{iso} = 1.2U_{equiv} of the parent atom (U_{iso} = 1.5 U_{equiv} for methyl). During the structure solution of **1c** and **2a**, electron density difference maps revealed that there was disordered solvent that could not be successfully modeled with or without restraints. Thus, the structure factors were modified using the PLATON SQUEEZE[117] technique, in order to produce a “solvate-free” structure factor set. For **1c**, PLATON reported a total electron density of 201 e^- and total solvent accessible volume of 771 $Å^3$, likely representing one pentane molecule per asymmetric unit. For **2a**, PLATON reported a total electron density of 334 e^- and total solvent accessible volume of 1477 $Å^3$. This corresponds to approximately one-half of a pentane molecule per asymmetric unit. In **2b**, the halide atoms were refined as a mixture of Cl and I. The relative occupancy was freely refined, converging at 86/14 for the major and minor conformations, respectively. Constraints were used on the thermal displacement parameters of the disordered atoms and restraints were used on Cl-Rh and I-Rh bonds in the minor

component of the disorder. Three independent sites of disorder were identified in **2e**. The relative occupancies of the sets of disordered atoms were freely refined, converging at major/minor ratios of 59/41 for the solvent disorder, 53/47 for the isopropyl disorder, and 92/8 for the chloride disorder. Constraints were used on the anisotropic displacement parameters of the disordered atoms. In **3c**, the THF solvent molecule and one of the mesityl groups were each found to be disordered over two positions. The relative occupancy of the two positions of each fragment was freely refined, converging at 68/32 for the major and minor conformations of the THF and 57/43 for the mesityl. Constraints were used on the thermal displacement parameters of the disordered atoms and restraints were used on bond lengths in the solvent. In **3d"**, one void space within the crystal was found to be partially occupied by a co-crystallized methyl iodide molecule. Its occupancy was freely refined, converging at 66%. In **4b-1**, the I and CH_3 substituents were disordered over two positions. The relative occupancy was freely refined, converging at 52/48 for the major and minor conformations, respectively. Constraints were used on the anisotropic displacement parameters of the disordered atoms. In **4e-*cis***, constraints were used on the anisotropic displacement parameters of the symmetry-disordered CH_2/Cl substituents.

■ ASSOCIATED CONTENT

Supporting information

The Supporting Information is available free of charge on the ACS Publications website at CCDC 1948889-1948897 contains the supplementary crystallographic data for this paper. These data can be obtained free of charge from The Cambridge Crystallographic Data Centre via www.ccdc.cam.ac.uk/structures. Detailed information about the X-ray structure determination and

additional discussion of computational modeling (PDF) and X-ray crystallographic data (CIF).

■ AUTHOR INFORMATION

Corresponding Author

*robert.smith.nielsen@gmail.com

*wag@caltech.edu

*tbg7h@virginia.edu

ORCID

Shunyan Gu: 0000-0002-3625-1042

Robert J. Nielsen: 0000-0002-7962-0186

Diane A. Dickie: 0000-0003-0939-3309

William A. Goddard III: 0000-0003-0097-5716

T. Brent Gunnoe: 0000-0001-5714-3887

Notes

The authors declare no competing financial interest.

■ ACKNOWLEDGEMENTS

The Gunnoe group acknowledges support from the U.S. National Science Foundation (1800173). The Goddard group acknowledges support from NSF (CBET-1805022).

■ References

1. Johansson Seechurn, C. C. C.; Kitching, M. O.; Colacot, T. J.; Snieckus, V. Palladium-Catalyzed Cross-Coupling: A Historical Contextual Perspective to the 2010 Nobel Prize. *Angew. Chem. Int. Ed.* **2012,** *51*, 5062-5085.

2. Jana, R.; Pathak, T. P.; Sigman, M. S. Advances in Transition Metal (Pd,Ni,Fe)-Catalyzed Cross-Coupling Reactions Using Alkyl-organometallics as Reaction Partners. *Chem. Rev.* **2011,** *111*, 1417-1492.

3. Miyaura, N.; Suzuki, A. Palladium-Catalyzed Cross-Coupling Reactions of Organoboron Compounds. *Chem. Rev.* **1995,** *95*, 2457-2483.

4. Tellis, J. C.; Primer, D. N.; Molander, G. A. Single-electron transmetalation in organoboron cross-coupling by photoredox/nickel dual catalysis. *Science* **2014,** *345*, 433-436.

5. Font, M.; Acuña-Parés, F.; Parella, T.; Serra, J.; Luis, J. M.; Lloret-Fillol, J.; Costas, M.; Ribas, X. Direct observation of two-electron Ag(I)/Ag(III) redox cycles in coupling catalysis. *Nature Communications* **2014,** *5*, 4373.

6. Ackermann, L.; Gunnoe, T. B., *Catalytic hydroarylation of carbon-carbon multiple bonds*. Wiley-VCH Verlag GmbH & Co. KGaA: Weinheim, 2018.

7. Ahlquist, M.; Nielsen, R. J.; Periana, R. A.; Goddard III, W. A. Product Protection, the Key to Developing High Performance Methane Selective Oxidation Catalysts. *J. Am. Chem. Soc.* **2009,** *131*, 17110-17115.

8. Gol'dshleger, N. F.; Shteinma, A. A.; Shilov, A. E.; Eskova, V. V. Reactions of alkanes in solutions of chloride complexes of platinum. *Russ. J. Phys. Chem.* **1972,** *46*, 785-786.

9. Muehlhofer, M.; Strassner, T.; Herrmann, W. A. New catalyst systems for the catalytic conversion of methane into methanol. *Angew. Chem. Int. Ed.* **2002,** *41*, 1745-1747.

10. Lin, M.; Sen, A. Direct catalytic conversion of methane to acetic acid in an aqueous medium. *Nature* **1994,** *368*, 613-615.

11. Wong-Foy, A. G.; Bhalla, G.; Liu, X. Y.; Periana, R. A. Alkane C−H Activation and Catalysis by an O-Donor Ligated Iridium Complex. *J. Am. Chem. Soc.* **2003,** *125*, 14292-14293.

12. Luinstra, G. A.; Labinger, J. A.; Bercaw, J. E. Mechanism and stereochemistry for nucleophilic attack at carbon of platinum (IV) alkyls: Model reactions for hydrocarbon oxidation with aqueous platinum chlorides. *J. Am. Chem. Soc.* **1993,** *115*, 3004-3005.

13. Periana, R. A.; Taube, D. J.; Evitt, E. R.; Löffler, D. G.; Wentrcek, P. R.; Voss, G.; Masuda, T. A mercury-catalyzed, high-yield system for the oxidation of methane to methanol. *Science* **1993,** *259*,

340-343.

14. Periana, R. A.; Taube, D. J.; Gamble, S.; Taube, H.; Satoh, T.; Fujii, H. Platinum catalysts for the high-yield oxidation of methane to a methanol derivative. *Science* **1998,** *280*, 560-564.

15. Stahl, S. S.; Labinger, J. A.; Bercaw, J. E. Homogeneous oxidation of alkanes by electrophilic late transition metals. *Angew. Chem. Int. Ed.* **1998,** *37*, 2180-2192.

16. Periana, R. A.; Mironov, O.; Taube, D.; Bhalla, G.; Jones, C. J. Catalytic, oxidative condensation of CH4 to CH3COOH in one step via CH activation. *Science* **2003,** *301*, 814-818.

17. Olah, G. A.; Molnár, Á., *Hydrocarbon chemistry*. John Wiley & Sons: 2003.

18. Caballero, A.; Pérez, P. J. Methane as raw material in synthetic chemistry: The final frontier. *Chem. Soc. Rev.* **2013,** *42*, 8809-8820.

19. Munz, D.; Strassner, T. Alkane C–H functionalization and oxidation with molecular oxygen. *Inorg. Chem.* **2015,** *54*, 5043-5052.

20. Goldberg, K. I.; Goldman, A. S. Large-scale selective functionalization of alkanes. *Acc. Chem. Res.* **2017,** *50*, 620-626.

21. Gol'dshleger, N. F.; Tyabin, M. B.; Shilov, A. E.; Shteinman, A. A. Activation of Saturated Hydrocarbons-Deuterium-Hydrogen Exchange in Solutions of Transition Metal Complexes. *Russ. J. Phys. Chem.* **1969,** *43*, 1222-1223.

22. Shilov, A. E.; Shul'pin, G. B. Activation of C−H bonds by metal complexes. *Chem. Rev.* **1997,** *97*, 2879-2932.

23. Jones, C. J.; Taube, D.; Ziatdinov, V. R.; Periana, R. A.; Nielsen, R. J.; Oxgaard, J.; Goddard III, W. A. Selective Oxidation of Methane to Methanol Catalyzed, with C−H Activation, by Homogeneous, Cationic Gold. *Angew. Chem.* **2004,** *116*, 4726-4729.

24. Gretz, E.; Oliver, T. F.; Sen, A. Carbon-hydrogen bond activation by electrophilic transition-metal compounds. Palladium(II)-mediated oxidation of arenes and alkanes including methane. *J. Am. Chem. Soc.* **1987,** *109*, 8109-8111.

25. Zimmermann, T.; Soorholtz, M.; Bilke, M.; Schüth, F. Selective Methane Oxidation Catalyzed by Platinum Salts in Oleum at Turnover Frequencies of Large-Scale Industrial Processes. *J. Am. Chem. Soc.* **2016,** *138*, 12395-12400.

26. Bhalla, G.; Periana, R. A. C–H Activation of Alkanes and Arenes Catalyzed by an O-Donor Bis(tropolonato)iridium(III) Complex. *Angew. Chem. Int. Ed.* **2005,** *44*, 1540-1543.

27. Jones, C. J.; Taube, D.; Ziatdinov, V. R.; Periana, R. A.; Nielsen, R. J.; Oxgaard, J.; Goddard III, W. A. Selective Oxidation of Methane to Methanol Catalyzed, with C–H Activation, by Homogeneous,

Cationic Gold. *Angew. Chem. Int. Ed.* **2004,** *43*, 4626-4629.

28. Kua, J.; Xu, X.; Periana, R. A.; Goddard III, W. A. Stability and Thermodynamics of the PtCl2 Type Catalyst for Activating Methane to Methanol: A Computational Study. *Organometallics* **2002,** *21*, 511-525.

29. Xu, X.; Kua, J.; Periana, R. A.; Goddard III, W. A. Structure, Bonding, and Stability of a Catalytica Platinum(II) Catalyst: A Computational Study. *Organometallics* **2003,** *22*, 2057-2068.

30. Oxgaard, J.; Tenn, W. J.; Nielsen, R. J.; Periana, R. A.; Goddard III, W. A. Mechanistic Analysis of Iridium Heteroatom C−H Activation: Evidence for an Internal Electrophilic Substitution Mechanism. *Organometallics* **2007,** *26*, 1565-1567.

31. Tenn, W. J.; Young, K. J. H.; Bhalla, G.; Oxgaard, J.; Goddard III, W. A.; Periana, R. A. CH Activation with an O-Donor Iridium−Methoxo Complex. *J. Am. Chem. Soc.* **2005,** *127*, 14172-14173.

32. Luinstra, G. A.; Wang, L.; Stahl, S. S.; Labinger, J. A.; Bercaw, J. E. C−H activation by aqueous platinum complexes: A mechanistic study. *J. Organomet. Chem.* **1995,** *504*, 75-91.

33. Arndtsen, B. A.; Bergman, R. G.; Mobley, T. A.; Peterson, T. H. Selective Intermolecular Carbon-Hydrogen Bond Activation by Synthetic Metal Complexes in Homogeneous Solution. *Acc. Chem. Res.* **1995,** *28*, 154-162.

34. Jones, W. D.; Feher, F. J. Comparative reactivities of hydrocarbon carbon-hydrogen bonds with a transition-metal complex. *Acc. Chem. Res.* **1989,** *22*, 91-100.

35. Kloek, S. M.; Heinekey, D. M.; Goldberg, K. I. C–H Bond Activation by Rhodium(I) Hydroxide and Phenoxide Complexes. *Angew. Chem.* **2007,** *119*, 4820-4822.

36. Janowicz, A. H.; Bergman, R. G. Carbon-hydrogen activation in completely saturated hydrocarbons: direct observation of M + R-H .fwdarw. M(R)(H). *J. Am. Chem. Soc.* **1982,** *104*, 352-354.

37. Jones, W. D.; Feher, F. J. Mechanism of arene carbon-hydrogen bond activation by (C5Me5)Rh(PMe3)(H)Ph. Evidence for arene precoordination. *J. Am. Chem. Soc.* **1982,** *104*, 4240-4242.

38. Vaughan, B. A.; Webster-Gardiner, M. S.; Cundari, T. R.; Gunnoe, T. B. A rhodium catalyst for single-step styrene production from benzene and ethylene. *Science* **2015,** *348*, 421-424.

39. Gunnoe, T. B., Metal-Mediated Carbon-Hydrogen Bond Activation. In *Physical Inorganic Chemistry: Reactions, Processes, and Applications*, Bakac, A., Ed. 2010.

40. Xu, H.-J.; Lu, Y.; Farmer, M. E.; Wang, H.-W.; Zhao, D.; Kang, Y.-S.; Sun, W.-Y.; Yu, J.-Q. Rh(III)-Catalyzed meta-C–H Olefination Directed by a Nitrile Template. *J. Am. Chem. Soc.* **2017,** *139*, 2200-

2203.

41. Colby, D. A.; Tsai, A. S.; Bergman, R. G.; Ellman, J. A. Rhodium Catalyzed Chelation-Assisted C–H Bond Functionalization Reactions. *Acc. Chem. Res.* **2012,** *45*, 814-825.

42. Cheng, C.; Hartwig, J. F. Rhodium-Catalyzed Intermolecular C–H Silylation of Arenes with High Steric Regiocontrol. *Science* **2014,** *343*, 853-857.

43. Frech, C. M.; Milstein, D. Direct Observation of Reductive Elimination of Methyl Iodide from a Rhodium(III) Pincer Complex: The Importance of Sterics. *J. Am. Chem. Soc.* **2006,** *128*, 12434-12435.

44. Feller, M.; Iron, M. A.; Shimon, L. J. W.; Diskin-Posner, Y.; Leitus, G.; Milstein, D. Competitive C−I versus C−CN Reductive Elimination from a RhIII Complex. Selectivity is Controlled by the Solvent. *J. Am. Chem. Soc.* **2008,** *130*, 14374-14375.

45. Feller, M.; Diskin-Posner, Y.; Leitus, G.; Shimon, L. J. W.; Milstein, D. Direct Observation of Reductive Elimination of MeX (X = Cl, Br, I) from RhIII Complexes: Mechanistic Insight and the Importance of Sterics. *J. Am. Chem. Soc.* **2013,** *135*, 11040-11047.

46. O'Reilly, M. E.; Pahls, D. R.; Webb, J. R.; Boaz, N. C.; Majumdar, S.; Hoff, C. D.; Groves, J. T.; Cundari, T. R.; Gunnoe, T. B. Reductive functionalization of a rhodium(III)–methyl bond by electronic modification of the supporting ligand. *Dalton Trans.* **2014,** *43*, 8273-8281.

47. O'Reilly, M. E.; Pahls, D. R.; Cundari, T. R.; Gunnoe, T. B. Reductive Functionalization of a Rhodium(III)–Methyl Bond in Acidic Media: Key Step in the Electrophilic Functionalization of Methane. *Organometallics* **2014,** *33*, 6504-6510.

48. Crabtree, R. H. Alkane C–H activation and functionalization with homogeneous transition metal catalysts: a century of progress—a new millennium in prospect. *J. Chem. Soc., Dalton Trans.* **2001**, 2437-2450.

49. Paulik, F. E.; Roth, J. F. Novel catalysts for the low-pressure carbonylation of methanol to acetic acid. *Chem. Commun. (London)* **1968**, 1578a-1578a.

50. Ojima, I.; Tsai, C.; Tzamarioudaki, M.; Bonafoux, D., The Hydroformylation Reaction. In *Organic Reactions*, 2004.

51. Forster, D. Kinetic and spectroscopic studies of the carbonylation of methanol with an iodide-promoted iridium catalyst. *J. Chem. Soc., Dalton Trans.* **1979**, 1639-1645.

52. Forster, D. On the mechanism of a rhodium-complex-catalyzed carbonylation of methanol to acetic acid. *J. Am. Chem. Soc.* **1976,** *98*, 846-848.

53. Van Leeuwen, P. W.; Claver, C., *Rhodium catalyzed hydroformylation*. Springer Science &

Business Media: 2002.

54. Low, J. J.; Goddard III, W. A. Theoretical studies of oxidative addition and reductive elimination. 2. Reductive coupling of hydrogen-hydrogen, hydrogen-carbon, and carbon-carbon bonds from palladium and platinum complexes. *Organometallics* **1986,** *5*, 609-622.

55. Furuya, T.; Benitez, D.; Tkatchouk, E.; Strom, A. E.; Tang, P.; Goddard III, W. A.; Ritter, T. Mechanism of C−F Reductive Elimination from Palladium(IV) Fluorides. *J. Am. Chem. Soc.* **2010,** *132*, 3793-3807.

56. Hartwig, J. F.; Collman, J. P., *Organotransition metal chemistry: from bonding to catalysis*. University Science Books Sausalito, CA: 2010.

57. Collman, J. P.; Hegedus, L. S.; Norton, J. R.; Finke, R. G., Principles and Applications of Organotransition Metal Chemistry. Elsevier: 1981.

58. Crabtree, R. H., Oxidative Addition and Reductive Elimination. In *The Organometallic Chemistry of the Transition Metals*, 2014.

59. Goldberg, K. I.; Yan, J. Y.; Winter, E. L. Competitive Carbon-Carbon Reductive Elimination and Carbon-Iodide Bond Formation from a Pt(IV) Complex. *J. Am. Chem. Soc.* **1994,** *116*, 1573-1574.

60. Racowski, J. M.; Gary, J. B.; Sanford, M. S. Carbon(sp3)–Fluorine Bond-Forming Reductive Elimination from Palladium(IV) Complexes. *Angew. Chem. Int. Ed.* **2012,** *51*, 3414-3417.

61. Mankad, N. P.; Toste, F. D. C(sp3)–F reductive elimination from alkylgold(iii) fluoride complexes. *Chemical Science* **2012,** *3*, 72-76.

62. Scott, V. J.; Labinger, J. A.; Bercaw, J. E. Mechanism of Reductive Elimination of Methyl Iodide from a Novel Gold(III)−Monomethyl Complex. *Organometallics* **2010,** *29*, 4090-4096.

63. Webster-Gardiner, M. S.; Fu, R.; Fortman, G. C.; Nielsen, R. J.; Gunnoe, T. B.; Goddard III, W. A. Arene C–H activation using Rh(I) catalysts supported by bidentate nitrogen chelates. *Catal. Sci. Technol.* **2015,** *5*, 96-100.

64. Fu, R.; O'Reilly, M. E.; Nielsen, R. J.; Goddard III, W. A.; Gunnoe, T. B. Rhodium Bis(quinolinyl)benzene Complexes for Methane Activation and Functionalization. *Chem. Eur. J.* **2015,** *21*, 1286-1293.

65. Webster-Gardiner, M. S.; Piszel, P. E.; Fu, R.; McKeown, B. A.; Nielsen, R. J.; Goddard III, W. A.; Gunnoe, T. B. Electrophilic RhI catalysts for arene H/D exchange in acidic media: Evidence for an electrophilic aromatic substitution mechanism. *J. Mol. Catal. A: Chem.* **2017,** *426*, 381-388.

66. Vaughan, B. A.; Khani, S. K.; Gary, J. B.; Kammert, J. D.; Webster-Gardiner, M. S.; McKeown, B. A.; Davis, R. J.; Cundari, T. R.; Gunnoe, T. B. Mechanistic Studies of Single-Step Styrene Production

Using a Rhodium(I) Catalyst. *J. Am. Chem. Soc.* **2017,** *139*, 1485-1498.

67. Webster-Gardiner, M. S.; Chen, J.; Vaughan, B. A.; McKeown, B. A.; Schinski, W.; Gunnoe, T. B. Catalytic Synthesis of “Super” Linear Alkenyl Arenes Using an Easily Prepared Rh(I) Catalyst. *J. Am. Chem. Soc.* **2017,** *139*, 5474-5480.

68. Chen, J.; Nielsen, R. J.; Goddard III, W. A.; McKeown, B. A.; Dickie, D. A.; Gunnoe, T. B. Catalytic Synthesis of Superlinear Alkenyl Arenes Using a Rh(I) Catalyst Supported by a “Capping Arene” Ligand: Access to Aerobic Catalysis. *J. Am. Chem. Soc.* **2018,** *140*, 17007-17018.

69. Zhu, W.; Luo, Z.; Chen, J.; Liu, C.; Yang, L.; Dickie, D. A.; Liu, N.; Zhang, S.; Davis, R. J.; Gunnoe, T. B. Mechanistic Studies of Single-Step Styrene Production Catalyzed by Rh Complexes with Diimine Ligands: An Evaluation of the Role of Ligands and Induction Period. *ACS Catal.* **2019,** *9*, 7457-7475.

70. Liebov, N. S.; Zhu, W.; Chen, J.; Webster-Gardiner, M. S.; Schinski, W. L.; Gunnoe, T. B. Rhodium-Catalyzed Alkenylation of Toluene Using 1-Pentene: Regioselectivity To Generate Precursors for Bicyclic Compounds. *Organometallics* **2019,** *38*, 3860-3870.

71. Wang, D. Y.; Choliy, Y.; Haibach, M. C.; Hartwig, J. F.; Krogh-Jespersen, K.; Goldman, A. S. Assessment of the Electronic Factors Determining the Thermodynamics of “Oxidative Addition” of C–H and N–H Bonds to Ir(I) Complexes. *J. Am. Chem. Soc.* **2016,** *138*, 149-163.

72. Krogh-Jespersen, K.; Czerw, M.; Zhu, K.; Singh, B.; Kanzelberger, M.; Darji, N.; Achord, P. D.; Renkema, K. B.; Goldman, A. S. Combined Computational and Experimental Study of Substituent Effects on the Thermodynamics of H2, CO, Arene, and Alkane Addition to Iridium. *J. Am. Chem. Soc.* **2002,** *124*, 10797-10809.

73. Albrecht, M.; van Koten, G. Platinum group organometallics based on “pincer” complexes: sensors, switches, and catalysts. *Angew. Chem. Int. Ed.* **2001,** *40*, 3750-3781.

74. Choi, J.; MacArthur, A. H. R.; Brookhart, M.; Goldman, A. S. Dehydrogenation and Related Reactions Catalyzed by Iridium Pincer Complexes. *Chem. Rev.* **2011,** *111*, 1761-1779.

75. Goldberg, J. M.; Wong, G. W.; Brastow, K. E.; Kaminsky, W.; Goldberg, K. I.; Heinekey, D. M. The importance of steric factors in iridium pincer complexes. *Organometallics* **2015,** *34*, 753-762.

76. Goldberg, J. M.; Cherry, S. D. T.; Guard, L. M.; Kaminsky, W.; Goldberg, K. I.; Heinekey, D. M. Hydrogen Addition to (pincer)IrI(CO) Complexes: The Importance of Steric and Electronic Factors. *Organometallics* **2016,** *35*, 3546-3556.

77. Anderson, B. G.; Spencer, J. L. The Coordination Chemistry of Pentafluorophenylphosphino Pincer Ligands to Platinum and Palladium. *Chem. Eur. J.* **2014,** *20*, 6421-6432.

78. Gruver, B. C.; Adams, J. J.; Warner, S. J.; Arulsamy, N.; Roddick, D. M. Acceptor Pincer Chemistry of Ruthenium: Catalytic Alkane Dehydrogenation by (CF3PCP)Ru(cod)(H). *Organometallics* **2011,** *30*, 5133-5140.

79. Adams, J. J.; Arulsamy, N.; Roddick, D. M. Acceptor PCP Pincer Iridium(I) Chemistry: Stabilization of Nonmeridional PCP Coordination Geometries. *Organometallics* **2011,** *30*, 697-711.

80. Guzei, I. A.; Wendt, M. An improved method for the computation of ligand steric effects based on solid angles. *Dalton Trans.* **2006**, 3991-3999.

81. Feller, M.; Ben-Ari, E.; Gupta, T.; Shimon, L. J. W.; Leitus, G.; Diskin-Posner, Y.; Weiner, L.; Milstein, D. Mononuclear Rh(II) PNP-Type Complexes. Structure and Reactivity. *Inorg. Chem.* **2007,** *46*, 10479-10490.

82. Hahn, C.; Sieler, J.; Taube, R. Synthesis of 2,6-bis(diphenylphosphinomethyl)pyridine-monoligand-rhodium(I) complexes [Rh(PNP)L]X with L = pyridine, CH3CN, DMSO and X = CF3SO3, BF4 from the corresponding ethylene complex and comparison of the structures to the piperidine complex (Lc= piperidine, X= BF4). *Polyhedron* **1998,** *17*, 1183-1193.

83. Hermann, D.; Gandelman, M.; Rozenberg, H.; Shimon, L. J. W.; Milstein, D. Synthesis, Structure, and Reactivity of New Rhodium and Iridium Complexes, Bearing a Highly Electron-Donating PNP System. Iridium-Mediated Vinylic C−H Bond Activation. *Organometallics* **2002,** *21*, 812-818.

84. Brown, T. H.; Green, P. J. Phosphorus-31 and rhodium-103 nuclear magnetic resonance spectra of some rhodium(I) and rhodium(III) phosphine complexes. *J. Am. Chem. Soc.* **1970,** *92*, 2359-2362.

85. Nixon, J. F.; Pidcock, A., Phosphorus-31 Nuclear Magnetic Resonance Spectra of Co-ordination Compounds. In *Annual Reports on NMR Spectroscopy*, Mooney, E. F., Ed. Academic Press: 1969; Vol. 2, pp 345-422.

86. Goldberg, K. I.; Yan, J.; Breitung, E. M. Energetics and Mechanisms of Carbon-Carbon and Carbon-Iodide Reductive Elimination from a Pt(IV) Center. *J. Am. Chem. Soc.* **1995,** *117*, 6889-6896.

87. Gair, J. J.; Qiu, Y.; Chan, N. H.; Filatov, A. S.; Lewis, J. C. Rhodium Complexes of 2,6-Bis(dialkylphosphinomethyl)pyridines: Improved C–H Activation, Expanded Reaction Scope, and Catalytic Direct Arylation. *Organometallics* **2017,** *36*, 4699-4706.

88. Separate entropy and enthalpy of activation are not computed because solvation free energies predicted by continuum models do not separate electrostatic stabilization of solutes (enthalpy) from the solvent reorganization and changes in dynamics upon solvation (entropy).

89. Heaton, B., *Mechanisms in homogeneous catalysis: a spectroscopic approach*. John Wiley & Sons: 2006.

90. Pidcock, A. Coupling and “virtual” coupling in the nuclear magnetic resonance spectra of phosphine complexes. *Chem. Commun. (London)* **1968**, 92.

91. Liou, S.-Y.; Gozin, M.; Milstein, D. Directly observed oxidative addition of a strong carbon-carbon bond to a soluble metal complex. *J. Am. Chem. Soc.* **1995,** *117*, 9774-9775.

92. Okazaki, M.; Tobita, H.; Kawano, Y.; Inomata, S.; Ogino, H. Thermal reactions of alkyl(hydrido)(hydrosilyl)iridium(III) complexes: generation of a hydrido(silylene)iridium(I) species via the reductive elimination of alkane and 1,2-H-shift from the silicon atom to the Ir(I) metal center. *J. Organomet. Chem.* **1998,** *553*, 1-13.

93. Montag, M.; Leitus, G.; Shimon, L. J. W.; Ben-David, Y.; Milstein, D. Solvent-Dependent Interconversions between RhI, RhII, and RhIII Complexes of an Aryl–Monophosphine Ligand. *Chem. Eur. J.* **2007,** *13*, 9043-9055.

94. Lipke, M. C.; Neumeyer, F.; Tilley, T. D. Interconversion of η3-H2SiRR′ σ-Complexes and 16-Electron Silylene Complexes via Reversible H–H or C–H Elimination. *J. Am. Chem. Soc.* **2014,** *136*, 6092-6102.

95. Zhou, M.; Goldman, A. S. Chlorination of (Phebox)Ir(mesityl)(OAc) by Thionyl Chloride. *Molecules* **2015,** *20*, 10122-10130.

96. Gabi, M.; Martti, K.; Markku, L.; Bernhard, R. Iron and Cobalt Complexes of a Series of Tridentate P, N, P Ligands — Synthesis, Characterization, and Application in Ethene Polymerization Reactions. *Z. Anorg. Allg. Chem.* **2002,** *628*, 2839-2846.

97. Ammann, C.; Meier, P.; Merbach, A. E. A simple multinuclear NMR thermometer. *J. Magn. Reson.* **1982,** *46*, 319-321.

98. Shih, W.-C.; Ozerov, O. V. One-Pot Synthesis of 1,3-Bis(phosphinomethyl)arene PCP/PNP Pincer Ligands and Their Nickel Complexes. *Organometallics* **2015,** *34*, 4591-4597.

99. Jacob, N.; Saravanakumar, E.; Anke, S.; Kathrin, J.; Matthias, B. Improved and General Manganese-Catalyzed N-Methylation of Aromatic Amines Using Methanol. *Chem. Eur. J.* **2017,** *23*, 5410-5413.

100. Cramer, R.; McCleverty, J. A.; Bray, J., Di-μ-chlorotetrakis(ethylene)dirhodium(I), 2,4-Pentanedionatobis(ethylene)rhodium(I), and Di-μ-chlorotetracarbonyldirhodium(I). In *Inorg. Synth.*, Parshall, G. W., Ed. 1974.

101. Becke, A. D. Density-Functional Thermochemistry: 3. The Role of Exact Exchange. *J. Chem. Phys.* **1993,** *98*, 5648-5652.

102. Grimme, S.; Antony, J.; Ehrlich, S.; Krieg, H. A consistent and accurate ab initio

parametrization of density functional dispersion correction (DFT-D) for the 94 elements H-Pu. *J. Chem. Phys.* **2010,** *132*, 154104.

103. Clark, T.; Chandrasekhar, J.; Spitznagel, G. W.; Schleyer, P. V. R. Efficient diffuse function-augmented basis sets for anion calculations. III. The 3-21+ G basis set for first-row elements, Li–F. *J. Comput. Chem.* **1983,** *4*, 294-301.

104. Frisch, M. J.; Pople, J. A.; Binkley, J. S. Self-consistent molecular orbital methods 25. Supplementary functions for Gaussian basis sets. *J. Chem. Phys.* **1984,** *80*, 3265-3269.

105. Peterson, K. A.; Figgen, D.; Goll, E.; Stoll, H.; Dolg, M. Systematically convergent basis sets with relativistic pseudopotentials. II. Small-core pseudopotentials and correlation consistent basis sets for the post-d group 16–18 elements. *J. Chem. Phys.* **2003,** *119*, 11113.

106. Hay, P. J.; Wadt, W. R. Ab Initio Effective Core Potentials for Molecular Calculations - Potentials for K to Au Including the Outermost Core Orbitals. *J. Chem. Phys.* **1985,** *82*, 299-310.

107. Zhao, Y.; Truhlar, D. G. A new local density functional for main-group thermochemistry, transition metal bonding, thermochemical kinetics, and noncovalent interactions. *J. Chem. Phys.* **2006,** *125*, 194101.

108. Tannor, D. J.; Marten, B.; Murphy, R.; Friesner, R. A.; Sitkoff, D.; Nicholls, A.; Honig, B.; Ringnalda, M.; Goddard III, W. A. Accurate first principles calculation of molecular charge distributions and solvation energies from ab initio quantum mechanics and continuum dielectric theory. *J. Am. Chem. Soc.* **1994,** *116*, 11875-11882.

109. Martin, J. M.; Sundermann, A. Correlation consistent valence basis sets for use with the Stuttgart–Dresden–Bonn relativistic effective core potentials: The atoms Ga–Kr and In–Xe. *J. Chem. Phys.* **2001,** *114*, 3408-3420.

110. Lee, C.; Yang, W.; Parr, R. G. Development of the Colle-Salvetti correlation-energy formula into a functional of the electron density. *Phys. Rev. B* **1988,** *37*, 785-789.

111. Hehre, W. J.; Ditchfield, R.; Pople, J. A. Self-Consistent Molecular-Orbital Methods: 12. Further Extensions of Gaussian-Type Basis Sets for Use in Molecular-Orbital Studies of Organic Molecules. *J. Chem. Phys.* **1972,** *56*, 2257-2261.

112. Francl, M. M.; Pietro, W. J.; Hehre, W. J.; Binkley, J. S.; Gordon, M. S.; DeFrees, D. J.; Pople, J. A. Self-consistent molecular orbital methods. XXIII. A polarization-type basis set for second-row elements. *J. Chem. Phys.* **1982,** *77*, 3654-3665.

113. Bochevarov, A. D.; Harder, E.; Hughes, T. F.; Greenwood, J. R.; Braden, D. A.; Philipp, D. M.; Rinaldo, D.; Halls, M. D.; Zhang, J.; Friesner, R. A. Jaguar: A high-performance quantum chemistry

software program with strengths in life and materials sciences. *Int. J. Quantum Chem* **2013,** *113*, 2110-2142.

114. Bruker *Saint; SADABS; APEX3*, Bruker AXS Inc.: Madison, Wisconsin, USA., 2012.

115. Sheldrick, G. SHELXT - Integrated space-group and crystal-structure determination. *Acta Crystallogr. Sect. A: Found. Crystallogr.* **2015,** *71*, 3-8.

116. Dolomanov, O. V.; Bourhis, L. J.; Gildea, R. J.; Howard, J. A. K.; Puschmann, H. OLEX2: a complete structure solution, refinement and analysis program. *J. Appl. Crystallogr.* **2009,** *42*, 339-341.

117. Spek, A. PLATON SQUEEZE: a tool for the calculation of the disordered solvent contribution to the calculated structure factors. *Acta Crystallogr. Sect. C: Cryst. Struct. Commun.* **2015,** *71*, 9-18.